NeuroImage 197 (2019) 716–741

Contents lists available at ScienceDirect

NeuroImage

journal homepage: www.elsevier.com/locate/neuroimage

Cortical layers: Cyto-, myelo-, receptor- and synaptic architecture in human cortical areas

Nicola Palomero-Gallagher [a,b,c,*], Karl Zilles [a,b,c,**]

[a] Institute of Neuroscience and Medicine (INM-1), Research Centre Jülich, Jülich, Germany
[b] Department of Psychiatry, Psychotherapy, and Psychosomatics, Medical Faculty, RWTH Aachen, Aachen, Germany
[c] JARA - Translational Brain Medicine, Aachen, Germany

ARTICLE INFO

Keywords:
Cerebral cortex
Cortical layers
Isocortex
Allocortex
Motor cortex
Sensory cortex
Association cortex
Transmitter receptors
Cytoarchitecture
Myeloarchitecture
Synaptic density

ABSTRACT

Cortical layers have classically been identified by their distinctive and prevailing cell types and sizes, as well as the packing densities of cell bodies or myelinated fibers. The densities of multiple receptors for classical neurotransmitters also vary across the depth of the cortical ribbon, and thus determine the neurochemical properties of cyto- and myeloarchitectonic layers. However, a systematic comparison of the correlations between these histologically definable layers and the laminar distribution of transmitter receptors is currently lacking. We here analyze the densities of 17 different receptors of various transmitter systems in the layers of eight cytoarchitectonically identified, functionally (motor, sensory, multimodal) and hierarchically (primary and secondary sensory, association) distinct areas of the human cerebral cortex. Maxima of receptor densities are found in different layers when comparing different cortical regions, i.e. laminar receptor densities demonstrate differences in receptorarchitecture between isocortical areas, notably between motor and primary sensory cortices, specifically the primary visual and somatosensory cortices, as well as between allocortical and isocortical areas. Moreover, considerable differences are found between cytoarchitectonical and receptor architectonical laminar patterns. Whereas the borders of cyto- and myeloarchitectonic layers are well comparable, the laminar profiles of receptor densities rarely coincide with the histologically defined borders of layers. Instead, highest densities of most receptors are found where the synaptic density is maximal, i.e. in the supragranular layers, particularly in layers II–III. The entorhinal cortex as an example of the allocortex shows a peculiar laminar organization, which largely deviates from that of all the other cortical areas analyzed here.

1. Introduction

Distinct layers of nerve cell bodies or myelinated axons parallel to the cortical surface were identified more than 175 years ago in the cerebral cortex. Six distinct layers were first described by Baillarger (1840). He made his observations in thin tissue sections without a microscope, and in the absence of any histological staining. He could identify alternating dark and white layers with the naked eye, or with a loupe under direct light. In transmitted light, he observed that the former white layers appear dark, and the dark layers light. Thus, he first described the intracortical layers containing densely packed myelinated fibers running parallel to the cortical surface as white stripes in direct light, and dark stripes in transmitted light, respectively (Fig. 1). Berlin (1858) microscopically identified six layers consisting of cell bodies of different shape and size using chromic acid and carmine staining. Notably, he could identify radially oriented fiber bundles, and cell dense as well as cell sparse layers (Fig. 2). In contrast to modern terminology, his layer 6 is nowadays called layer I, and our innermost cortical layer VI is his layer 1. Additionally, he identified large pyramidal cells in layer V (his layer 2).

With the advent of myelin and cell body staining techniques around the end of the 19th century, the analysis of cortical layering resulted in several classical monographies on the cerebral cortex (e.g., Brodmann, 1909; Vogt and Vogt, 1919; von Economo and Koskinas, 1925). The different cortical layers were microscopically defined by differences in their prevailing cell types (pyramidal cells versus "granular" cells), packing density of cell bodies, or of myelinated fibers. This led to layering schemes of the cerebral cortex (Fig. 3), and the delineation of numerous cortical regions ("areas") based on cell body staining (cytoarchitecture), or myelin staining (myeloarchitecture) techniques. This work was done by serial sectioning of entire human and non-human postmortem brains

* Corresponding author. Institute of Neuroscience and Medicine (INM-1), Research Centre Jülich, 52425 Jülich, Germany.
** Corresponding author. Institute of Neuroscience and Medicine (INM-1), Research Centre Jülich, 52425 Jülich, Germany.
E-mail addresses: n.palomero-gallagher@fz-juelich.de (N. Palomero-Gallagher), k.zilles@fz-juelich.de (K. Zilles).

http://dx.doi.org/10.1016/j.neuroimage.2017.08.035
Received 24 April 2017; Received in revised form 8 August 2017; Accepted 11 August 2017
Available online 12 August 2017

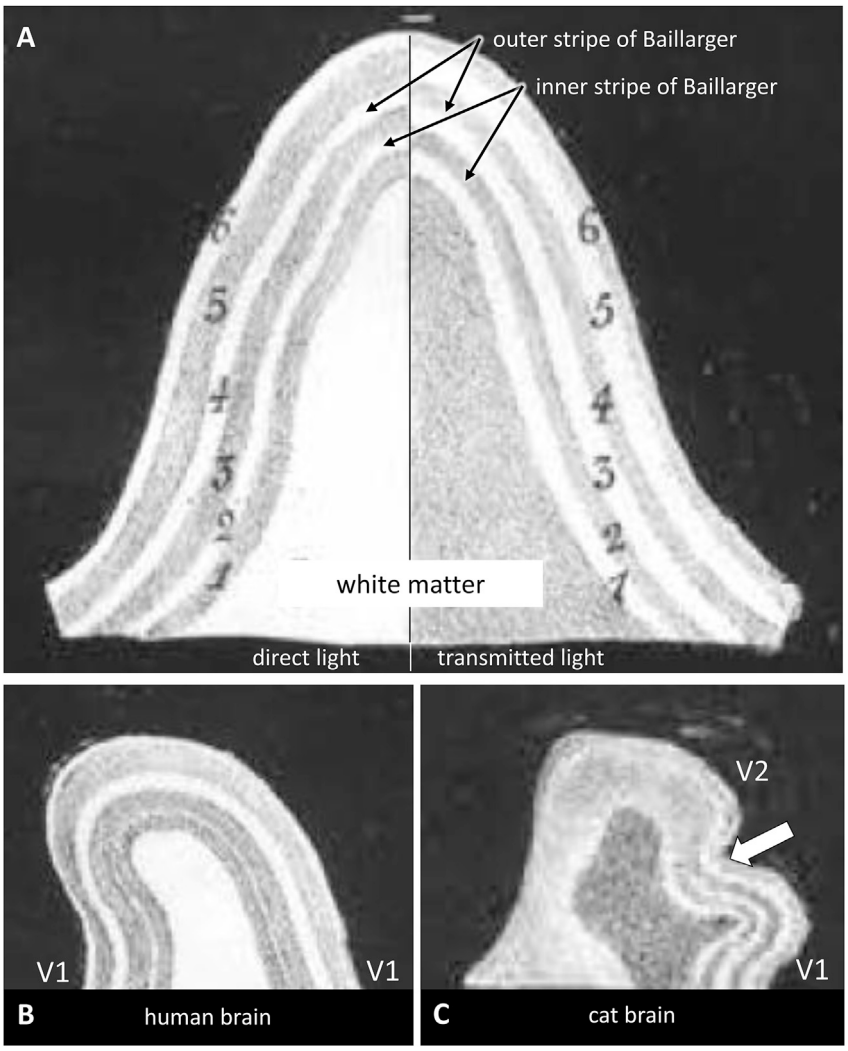

Fig. 1. Illustrations of cortical layers in sections through the isocortex by Baillarger (1840) using direct (A left) and transmitted (A right, B and C) light. A General isocortical laminar pattern, B Primary visual cortex V1, C Border (arrow) between primary (V1) and secondary (V2) visual cortex. Identifications of cortical areas and white inscriptions by the authors. Note the inverse sequence of the numbering of cortical layers by Baillarger (1840) compared with the modern nomenclature.

or of hemispheres in the coronal, horizontal (axial), or sagittal planes using microtomes, followed by histological staining and microscopic inspection (Brodmann, 1909; Vogt and Vogt, 1919), or by excision of smaller tissue blocks vertical to the cortical surface to avoid the more difficult analysis in oblique or tangential sections (von Economo and Koskinas, 1925). Although these studies resulted in comparable layering schemes, the parcellation of the cortex into numerous areas differ when using two modalities (cyto- versus myeloarchitecture), or even within a single modality. This led to severe criticism of this approach (Bailey and von Bonin, 1951; Lashley and Clark, 1946), and the conclusion of a lack of reproducibility of cyto- and myeloarchitectonic mapping. Therefore, quantitative cytoarchitecture has been introduced which is based on statistically testable identifications of borders between cortical areas (Amunts et al., 1999; Palomero-Gallagher and Zilles, 2017; Schleicher et al., 2005; Zilles et al., 2002b). This method also enables a continuous measurement of cell and receptor densities from the cortical surface to the cortex/white matter boundary and, thus, quantitatively based delineations of layers (Schleicher et al., 2000).

Transmitter receptors play a key role in signal processing. Their varying density throughout the cortical depth results in a laminar pattern (Zilles et al., 2002b) which, at a first glance, is reminiscent of that found in the cyto- or myeloarchitectonically defined layering schemes of the isocortex (Brodmann, 1909; Vogt and Vogt, 1919; von Economo and Koskinas, 1925). However, the typical six-layered pattern of cytoarchitecture cannot be found in most receptor types; consequently, the borders between receptor-dense and receptor-sparse layers do not consistently coincide with the borders of layers detectable in cyto- or myeloarchitectonic studies. Rather, receptor densities seem to show a type- and region-specific layering pattern (Amunts et al., 2010; Caspers et al., 2013, 2015; Cortés et al., 1986, 1987; Eickhoff et al., 2007, 2008; Hoyer et al., 1986a,b; Jansen et al., 1989; Morosan et al., 2005; Palomero-Gallagher et al., 2008, 2009, 2013, 2015, Pazos et al., 1987a,b; Scheperjans et al., 2005a,b; Vogt et al., 2013; Zilles et al., 2002a, 2004, 2015a; Zilles and Amunts, 2009; Zilles and Palomero-Gallagher, 2001, 2017). Since most receptors are found on dendrites and not on the cell bodies of pyramidal cells and interneurons (Kooijmans et al., 2014), and the dendrites of pyramidal cells cross many cytoarchitectonically defined layers, the layering pattern of receptors is not bound to a single layer of cell bodies (cytoarchitecture) or myelinated nerve fibers (myeloarchitecture). Therefore, a multimodal comparison of cyto-, myelo- and receptorarchitecture can reveal the precise correlation of the different layering schemes.

The introduction of high-resolution MR-based imaging seems to open a way to study cortical lamination in vivo (Callaghan et al., 2014; Cohen-Adad et al., 2012; Deistung et al., 2013; Dick et al., 2012; Dinse et al., 2015; Geyer et al., 2011; Marques et al., 2017; Polimeni et al., 2010). This would enable to analyze a larger number of brains and thus reveal the interindividual variability of cortical layers. Further, quantitative

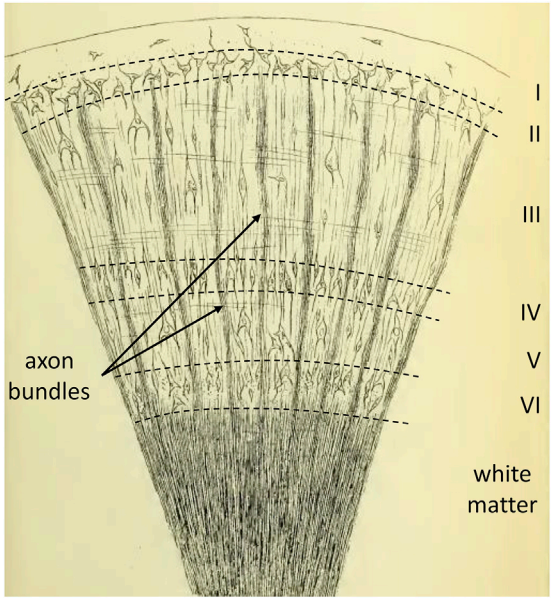

Fig. 2. Myelinated axonal fiber bundles and cell layers in the human isocortex. Illustration from Berlin (1858). Delineation and identification of cortical layers according to the modern cytoarchitectonic nomenclature by the authors.

measurements could be performed to obtain an objective analysis of architectonic differences between cortical areas, and the time-consuming analysis of histological sections could be avoided. However, the interpretation of the MR-based laminar pattern requires a comparison with the anatomical ground truth of the postmortem studies, since the identification of "layers" in the MR images poses the question whether these "layers" are identical with cyto- or myeloarchitectonically defined layers.

The aim of the present study is a comparison of the classical cyto- and myeloarchitectonic layering with that of multiple transmitter receptors in the human brain. Primary and secondary visual, primary somatosensory, motor, and limbic areas, as well as areas of multimodal association cortices are studied, since they show different layering patterns dependent on the staining or labeling technique. Detailed descriptions of the primary and secondary visual cortex (areas V1 and V2), primary somatosensory area 3b, primary motor cortex (area M1), area 44 of the Broca region, area 7 of the superior parietal lobule, anterior cingulate area 24 and of the entorhinal cortex have been reported (Amunts et al., 1999; Braak, 1972; Braak and Braak, 1992; Clarke and Miklossy, 1990; Jones, 1986; Lund et al., 1994; Palomero-Gallagher et al., 2008; Peters, 1994; Rockland, 1994; Scheperjans et al., 2008; von Economo and Koskinas, 1925; Zilles and Clarke, 1997). Areas were chosen to encompass brain regions from different evolutionary backgrounds (archicortex vs. neocortex), functional systems (sensory vs. motor; somatosensory vs. visual), and hierarchical processing levels (primary vs. early visual; unimodal vs. multimodal association). We will further compare the laminar distribution of the multiple receptors types with synaptic densities in the various layers of the cerebral cortex as reported in the literature. Finally, the question whether single cytoarchitectonical layers have similar multi-receptor expression patterns despite the diverse functional and structural cortical regions under consideration will

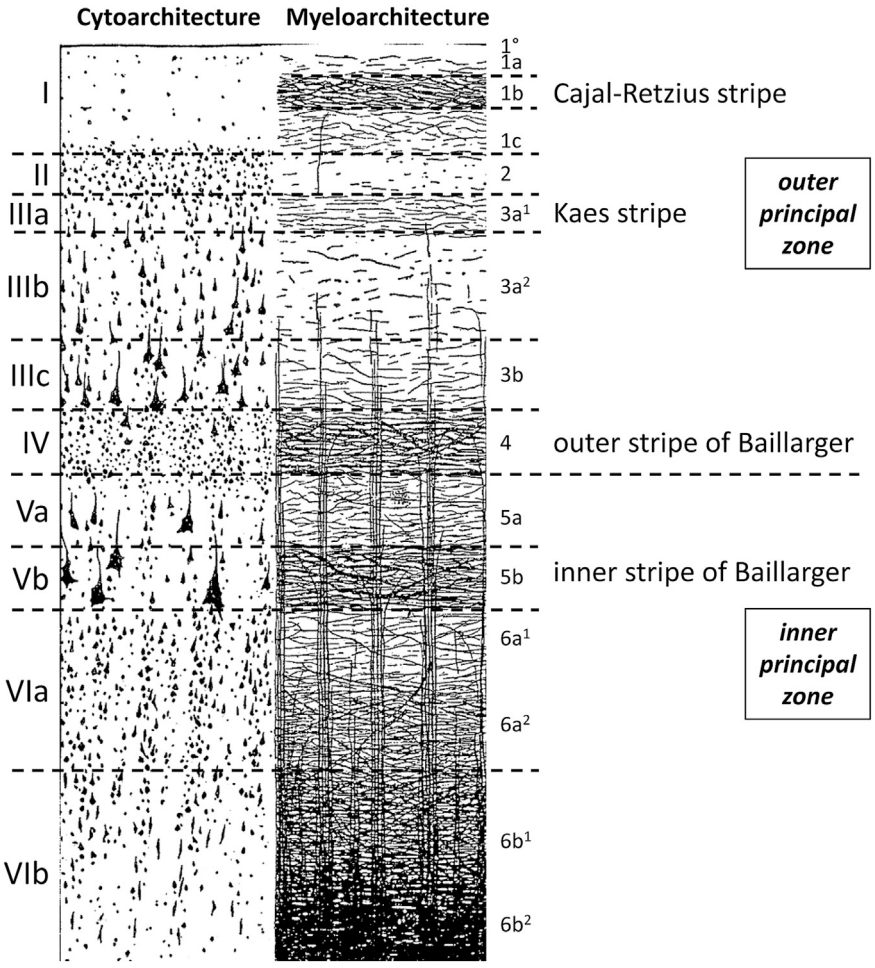

Fig. 3. Generalized scheme of cortical layering in cyto- and myeloarchitecture modified from Zilles et al. (Zilles et al., 2015b). Roman numbers cytoarchitectonic layers, Arabic numbers myeloarcitectonic layers.

be studied.

Laminar distribution patterns of transmitter receptors seem to be closely associated with cytoarchitectonical layering. However, the regional and laminar-specific differences in receptor densities do not simply reflect variations in cell packing densities as found in cytoarchitectonic studies. Rather, we hypothesize that receptor densities may indicate the laminar distribution of synapses. Furthermore, regional as well as laminar differences in cyto- and receptorarchitecture may correlate with their position in the hierarchies of the various functional networks, and their structural organization regarding classification into isocortical and allocortical areas.

2. Material and methods

Brains of four donors without a record of neurological or psychiatric diseases (age range: 67–77 years; 3 males, 1 female) were removed at autopsy. Post mortem delays were between 12 and 18 h before the brains were deep frozen. Details of pharmacological treatments were not available, but records of long-term drug treatment were not found. Causes of death were multiorgan failure caused by sepsis and pneumonia,

Table 1
Labelling protocols. $GABA_{A\ bz}$, $GABA_A$ associated benzodiazepine binding sites. * substance only included in the main incubation.

Receptor	Receptor characteristics	Ligand (pharmacological class) [nM]	Displacer [μm]	Incubation buffer	Pre-incubation	Main incubation	Final rinsing
AMPA	ionotropic, excitatory	[^{3}H]-AMPA (agonist) [10.0]	Quisqualate [10]	50 mM Tris-acetate (pH 7.2) +100 mM KSCN*	3 × 10 min, 4 °C	45 min, 4 °C	1) 4 × 4 s 2) Acetone/glutaraldehyde (100 ml + 2,5 ml), 2 × 2 s, 4 °C
NMDA	ionotropic, excitatory	[^{3}H]-MK-801 (antagonist) [3.3]	(+)MK-801 [100]	50 mM Tris-acetate (pH 7.2) +50 μM glutamate + 30 μM glycine* + 50 μM spermidine*	15 min, 4 °C	60 min, 22 °C	1) 2 × 5 min, 4 °C 2) distilled water, 1×, 22 °C
kainate	ionotropic, excitatory	[^{3}H]-Kainate (agonist) [9.4]	SYM 2081 [100]	50 mM Tris-acetate (pH 7.1) +10 mM Ca^{2+}-acetate*	3 × 10 min, 4 °C	45 min, 4 °C	1) 3 × 4 s 2) Acetone/glutaraldehyde (100 ml + 2,5 ml), 2 × 2 s, 22 °C
mGluR2/3	metabotropic, excitatory	[^{3}H]-LY 341,495 (antagonist) [1.0]	L-Glutamate [1000]	10 mM phosphate buffer (pH 7.6) +100 mM KBr*	2 × 5 min, 22 °C	60 min, 4 °C	1) 2 × 5 min 2) distilled water, 1×, 22 °C
$GABA_A$	ionotropic, inhibitory	[^{3}H]-Muscimol (agonist) [7.7]	GABA [10]	50 mM Tris-citrate (pH 7.0)	3 × 5 min, 4 °C	40 min, 4 °C	1) 3 × 3 s, 4 °C 2) distilled water, 1×, 22 °C
$GABA_{A\ bz}$	ionotropic, inhibitory	[^{3}H]-Flumazenil (antagonist) [1.0]	Clonazepam [2]	170 mM Tris-HCl (pH 7.4)	15 min, 4 °C	60 min, 4 °C	1) 2 × 1 min, 4 °C 2) distilled water, 1×, 22 °C
$GABA_B$	metabotropic, inhibitory	[^{3}H]-CGP 54626 (antagonist) [2.0]	CGP 55845 [100]	50 mM Tris-HCl (pH 7.2) +2,5 mM $CaCl_2$	3 × 5 min, 4 °C	60 min, 4 °C	1) 3 × 2 s, 4 °C 2) distilled water, 1×, 22 °C
M_1	metabotropic, excitatory	[^{3}H]-Pirenzepine (antagonist) [1.0]	Pirenzepine [2]	Modified Krebs buffer (pH 7.4)	15 min, 4 °C	60 min, 4 °C	1) 2 × 1 min, 4 °C 2) distilled water, 1 ×, 22 °C
M_2	metabotropic, inhibitory	[^{3}H]-Oxotremorine-M (agonist) [1.7]	Carbachol [10]	20 mM HEPES-Tris (pH 7.5) +10 mM $MgCl_2$ +300 nM Pirenzepine	20 min, 22 °C	60 min, 22 °C	1) 2 × 2 min, 4 °C 2) distilled water, 1 ×, 22 °C
M_3	metabotropic, excitatory	[^{3}H]-4-DAMP (antagonist) [1.0]	Atropine sulfate [10]	50 mM Tris-HCl (pH 7.4) +0.1 mM PSMF +1 mM EDTA	15 min, 22 °C	45 min, 22 °C	1) 2 × 5 min, 4 °C 2) distilled water, 1 ×, 22 °C
nicotinic $\alpha_4\beta_2$	ionotropic, excitatory	[^{3}H]-Epibatidine (agonist) [0.5]	Nicotine [100]	15 mM HEPES (pH 7.5) +120 mM NaCl +5.4 mM KCl +0.8 mM $MgCl_2$ +1.8 mM $CaCl_2$	20 min, 22 °C	90 min, 22 °C	1) 5 min, 4 °C 2) distilled water, 1 ×, 22 °C
α_1	metabotropic, excitatory	[^{3}H]-Prazosin (antagonist) [0.2]	Phentolamine Mesylate [10]	50 mM Na/K-phosphate buffer (pH 7.4)	15 min, 22 °C	60 min, 22 °C	1) 2 × 5 min, 4 °C 2) distilled water, 1 ×, 22 °C
α_2	metabotropic, inhibitory	[^{3}H]-UK 14,304 (agonist) [0.64]	Phentolamine Mesylate [10]	50 mM Tris-HCl (pH 7.7) +100 μM $MnCl_2$	15 min, 22 °C	90 min, 22 °C	1) 5 min, 4 °C 2) distilled water, 1 ×, 22 °C
5-HT_{1A}	metabotropic, inhibitory	[^{3}H]-8-OH-DPAT (agonist) [1.0]	5-Hydroxy-tryptamine, [1]	170 mM Tris-HCl (pH 7.4) +4 mM $CaCl_2$* +0.01% ascorbate*	30 min, 22 °C	60 min, 22 °C	1) 5 min, 4 °C 2) distilled water, 3 ×, 22 °C
5-HT_2	metabotropic, excitatory	[^{3}H]-Ketanserin (antagonist) [1.14]	Mianserin [10]	170 mM Tris-HCl (pH 7.7)	30 min, 22 °C	120 min, 22 °C	1) 2 × 10 min, 4 °C 2) distilled water, 3 ×, 22 °C
D_1	metabotropic, excitatory	[^{3}H]-SCH 23390 (antagonist) [1.67]	SKF 83566 [1]	50 mM Tris-HCl (pH 7.4) +120 mM NaCl +5 mM KCl +2 mM $CaCl_2$ +1 mM $MgCl_2$	20 min, 22 °C	90 min, 22 °C	1) 2 × 20 min, 4 °C 2) distilled water, 1 ×, 22 °C
A_1	metabotropic, inhibitory	[^{3}H]-DPCPX (antagonist) [1.0]	R-PIA [100]	170 mM Tris-HCl (pH 7.4) +2 Units/l Adenosine deaminase +100 μM Gpp(NH)p*	15 min, 4 °C	120 min, 22 °C	1) 2 × 5 min, 4 °C 2) distilled water, 1 ×, 22 °C

respiratory insufficiency, sudden cardiac failure, and lung edema. Each hemisphere was cut into approximately 3 cm thick slabs which were shock frozen in isopentane at −40 °C and stored at −80 °C in airtight plastic bags until further processing. Subjects had given written consent before death and/or had been included in the body donor program of the Department of Anatomy, University of Düsseldorf, Germany.

Unfixed frozen slabs were serially sectioned in the coronal plane (section thickness 20 μm) with a large scale cryostat microtome, and alternating sections were processed for quantitative *in vitro* receptor autoradiography (Palomero-Gallagher and Zilles, 2017; Zilles et al., 2002b), or for cell-body (Merker, 1983) or myelin (Gallyas, 1979) stainings. Multiple receptors for the classical neurotransmitters glutamate (AMPA, NMDA, kainate, mGluR2/3), GABA ($GABA_A$, $GABA_A$ associated benzodiazepine [$GABA_{A\ bz}$] binding sites, $GABA_B$), acetylcholine (muscarinic M_1, M_2, M_3, nicotinic $\alpha_4\beta_2$), noradrenaline (α_1, α_2), serotonin (5-HT_{1A}, 5-HT_2), and dopamine (D_1), as well as for adenosine (A_1) were labeled according to previously published receptor protocols consisting of pre-incubation, main incubation and rinsing steps (Table 1; Palomero-Gallagher and Zilles, 2017; Zilles et al., 2002b). In short, sections are rehydrated during the pre-incubation, and endogenous substances which could block the binding site for the tritiated ligand are removed. In the main incubation, sections are incubated in a buffer solution containing either the tritiated ligand or the tritiated ligand together with a non-labeled specific displacer. Incubation with the labeled ligand alone demonstrates its total binding, whereas incubation with the tritiated ligand and the displacer reveals the proportion of total binding sites which is occupied by non-specific binding. Thus, specific binding is the difference between total and non-specific binding, and amounted to 95% of total binding in the present study.

Radiolabelled sections were exposed against tritium-sensitive films (Hyperfilm, Amersham, Braunschweig, Germany) together with scales of known radioactivity concentrations (Microscales®, Amersham). The autoradiographs were digitized by means of a CCD-camera and the image acquisition and processing system Axiovision (Zeiss, Germany). The relationship between the gray value of a pixel in the digitized autoradiograph and the binding site concentration (i.e., the Bmax) which it encodes was defined first by a calibration curve computed based on the gray values derived from the plastic scales and their known concentrations of radioactivity, and then corrected to account for experimental conditions (e.g. specific activity, dissociation constant and free concentration of the ligand during incubation; see formula 1 and Palomero-Gallagher and Zilles, 2017; Zilles et al., 2002b). Thus, in the ensuing linearized autoradiographs, which can be color coded for visualization purposes, each pixel provides the receptor density in fmol/mg protein.

$$C_b = \frac{R}{E \cdot B \cdot W_b \cdot S_a} \cdot \frac{K_D + L}{L} \quad (1)$$

where R is the radioactivity concentration in counts per minute (cpm), C_b is Bmax and thus the binding site concentration in fmol/mg, E is the efficiency of the scintillation counter (depends on the actual counter), B is a constant representing the number of decays per unit of time and radioactivity (Ci/min), W_b the protein weight of a standard (mg), S_a the specific activity of the ligand (Ci/mmol), K_D the dissociation constant of the ligand (nM), and L the free concentration of the ligand during incubation (nM).

Equidistant receptor profiles oriented vertically to the cortical surface were extracted by means of a minimum length algorithm from the linearized autoradiographs (Schleicher et al., 2000). Receptor profiles quantify the receptor density from the pial surface to the border between layer VI and the white matter, and were obtained from regions of different cytoarchitecture. These receptor profiles were compared with the layering of cell bodies (cytoarchitecture) and myelinated nerve fibers (myeloarchitecture) visualized in alternating sections. The surface defined beneath a receptor profile, or beneath discrete sectors defined by the position of borders between cytoarchitectonic layers, can be computed to yield the absolute binding site densities for the entire cortical depth, or for cytoarchitectonically defined layers, in that particular area.

Specifically, we examined laminar distribution patterns of 17 different receptors in isocortical areas M1 (primary motor cortex, cytoarchitectonical area 4; Brodmann, 1909), 3b (primary somatosensory cortex; Jones, 1986), V1 (primary visual cortex, cytoarchitectonical area 17; Brodmann, 1909), V2 (secondary visual cortex, cytoarchitectonical area 18; Brodmann, 1909), 44v (receptorarchitectonically defined ventral portion of area 44 of Broca's region; Amunts et al., 2010), and 7A (cyto- and receptorarchitectonically identified association area of the superior parietal lobule; Scheperjans et al., 2005b, 2008), as well as in allocortical (periarchicortical) areas p24 (Palomero-Gallagher et al., 2008) and the entorhinal cortex (Stephan, 1975).

3. Results

The present observations are focused on a comparison of myelin and receptor distributions in layers of representative areas of the human cerebral cortex with classical cytoarchitectonic descriptions of their layering pattern.

3.1. Primary motor cortex (M1)

The primary motor cortex M1 is the functional equivalent of cytoarchitectonic area 4 (BA4; Brodmann, 1909) and myeloarchitectonic area V42 (Vogt and Vogt, 1919). It is a broad cortical ribbon of approximately 4.2–5.7 mm (shrinkage corrected; Zilles and Amunts, 2015) characterized by the occurrence of the giant pyramidal cells of Betz and a hardly visible c-layer IV (Fig. 4). The slightly higher cell density of layer II enables its delineation from layer III, which can be subdivided into the sublayers IIIa-IIIc. IIIb is less cell dense than IIIa, and IIIc contains somewhat larger pyramidal cells than IIIb. Layer V can be subdivided into sublayers Va and Vb, with the Betz cells in Vb. Also layer VI is heterogeneous, with a denser layer VIa than VIb.

In myelin stained sections, M1 appears to be heavily myelinated, and most important for MRI studies, the transition from the white matter to the cortical ribbon is only gradual (Figs. 4 and 5). Therefore, the real thickness of this area is sometimes underestimated by more than 50% in MRI studies (e.g., la Fougère et al., 2011), which are sensitive to myelin density. Whereas the borders between m-layers 1–3 are revealed by intermediate myelin densities in layers 1 and 3 separated by a low density in layer 2, m-layers 4–6 are hardly delineable from each other (Fig. 4). Notably, an m-layer 4 was delineated by Vogt and Vogt (1919) by a very weak outer Baillarger stripe (horizontally running fibers). Thus, m-layer 4 corresponds to the location of small granular cells (c-layer IV) as recently demonstrated (Barbas and Garcia-Cabezas, 2015; Garcia-Cabezas and Barbas, 2014). Layers 4–6 contain mostly vertically running fiber bundles, and m-layer 1 horizontally and obliquely oriented nerve fibers.

All examined receptors in M1 present a unimodal distribution pattern with by far the highest concentrations in the supragranular layers, particularly in c-layers I–IIIb (Fig. 5). After the maximum in the supragranular layers, some receptors ($GABA_A$, $GABA_{A\ bz}$, $GABA_B$, kainate, mGluR2/3, all cholinergic, 5-HT_{1A}, α_1, and α_2) show a sharp decline in direction to the deepest layers. In contrast, AMPA, NMDA, A_1, D_1, and 5-HT_2 receptors display a more shallow decrease starting from layer IIIc. Although local maxima of receptor densities can be assigned to c-layers, the borders of the c-layers do not coincide with a local maximum or minimum of the density profile. Consequently, the extension and localization of receptor fields do not indicate the precise localization of the borders between c-layers. Notably, most receptors, particularly the AMPA receptor, are visible at low densities in the white matter immediately below c-layer VIb (Fig. 5).

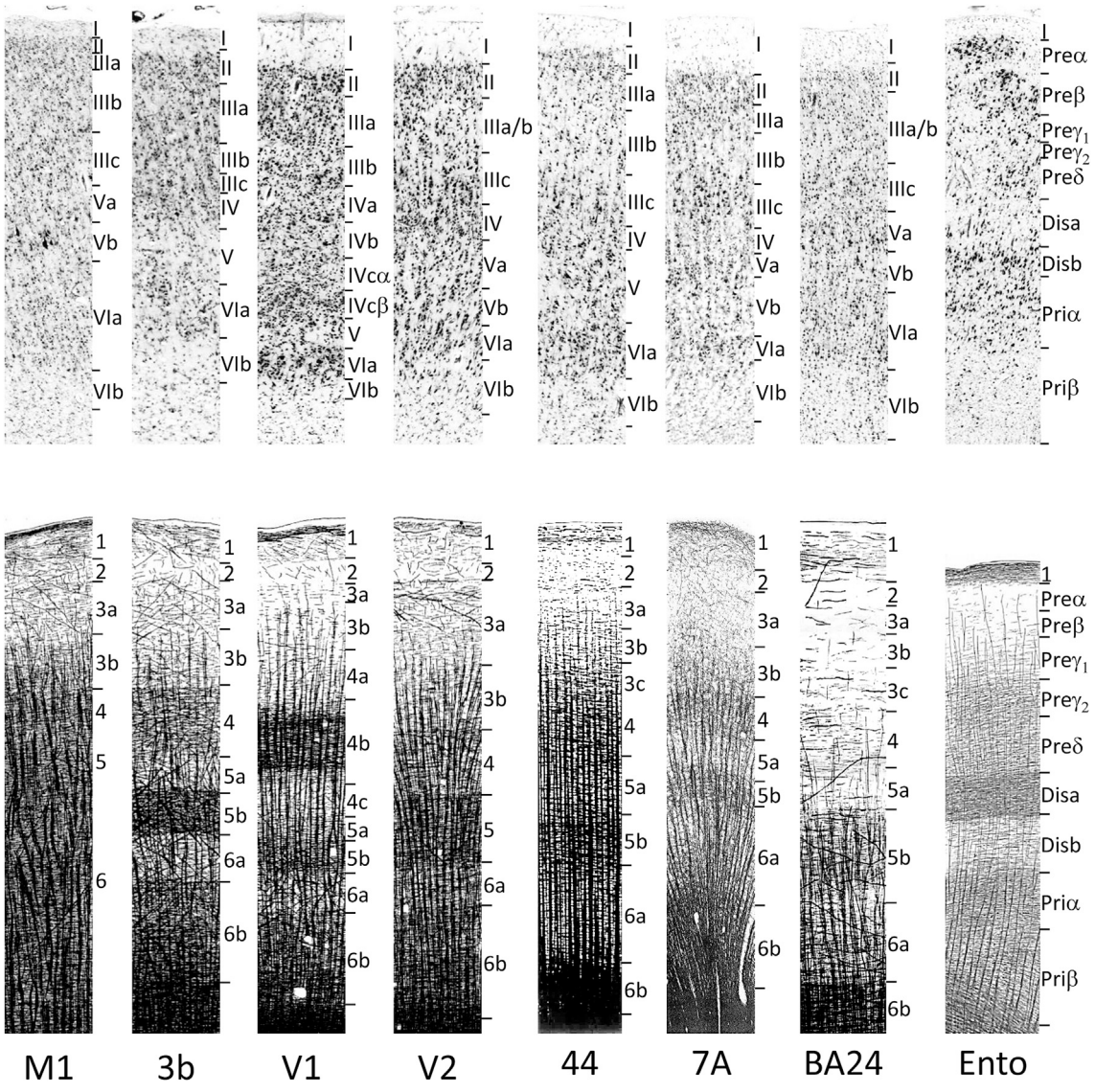

Fig. 4. Laminar patterns in cyto-(upper row) and myeloarchitecture (lower row). From left to right: primary motor cortex (area BA4/V42; illustration from Vogt and Vogt, 1919), primary somatosensory cortex (area BA3/V69; illustration from Vogt and Vogt, 1919), primary visual cortex (area BA17/Area striata; illustration from Vogt and Vogt, 1919), secondary visual cortex (BA18/Area occipitalis; illustration from Vogt and Vogt, 1919), multimodal association cortex of the inferior frontal gyrus (area BA44/V57; illustration from Vogt and Vogt, 1919), multimodal association cortex of the superior parietal lobule (area BA7/V83; illustration from Vogt, 1911), limbic cortex of the cingulate gyrus (area B24/V19; illustration from Vogt and Vogt, 1919); entorhinal cortex (area λ15d; illustration from Sgonina, 1937). BA nomenclature after Brodmann (1909), V nomenclature after Vogt and Vogt (1919) or Vogt (1911). The different absolute cortical thicknesses of the various areas have been normalized. Laminar borders were slightly modified by the authors for congruency regarding myeloarchitectonic details. The illustrations by Vogt (1911), Vogt and Vogt (1919), and Sgonina (1937) show more details than visible in routine myelin stained sections (Figs. 5–12) because Vogt and Vogt (1919) first hyperstained the sections and then differentiated the intensity by a careful destaining.

3.2. Primary somatosensory cortex (S1, area 3b)

The primary somatosensory cortex is much thinner than the primary motor cortex. It reaches a thickness of only 2.4–2.7 mm (shrinkage corrected; Zilles and Amunts, 2015). S1 is characterized by a typical koniocortical appearance with a conspicuously high cell density in c-layers II–IV (Fig. 4). Layer III is relatively broad, with numerous small pyramids, particularly at the border with layer II. An increasing number of isolated medium-sized pyramids appears in layer III when moving towards layer IV. This feature enables the delineation of sublayers IIIa-IIIc.

The myeloarchitecture of S1 is characterized by a dense outer Baillarger stripe (m-layer 4) and a very dense and clearly visible inner Baillarger stripe (m-layer 5b; Fig. 4). The levels of these stripes correspond to c-layers IV and V, respectively. Thus, the position and extent of c- and m-layers is well comparable. As in all isocortical areas, the vertical fiber bundles are not visible above m-layer 3b. The m-layer 3a/3b border is defined by this feature. More general, all borders between m-layers are demarcated in S1 by alternating higher and lower densities of myelin (Fig. 4).

Most receptors present a unimodal distribution in S1, with higher densities in the supragranular than in the infragranular c-layers (Fig. 6). Concentrations of $GABA_B$, AMPA, mGluR2/3, M_1, M_3, and α_1 receptors reach highest values in c-layers II–IIIa, gradually decrease through c-layers IIIb-IIIc, and show a plateau over c-layers IV–VIa. Lowest concentrations were measured in c-layer VIb. D_1 and 5-HT_{1A} receptors present a similar distribution, though their densities reach a plateau in c-layers IIIc and IIIb, respectively. Highest densities of $GABA_A$, $GABA_{A\ bz}$, NMDA, M_2, and 5-HT_2 receptor binding sites are found in c-layers IIIa and IIIb. Furthermore, since the decrease in receptor densities when moving towards the c-layer VI/white matter border is gradual, they do not show a plateau at the level of c-layers IV and V. Adrenergic α_2

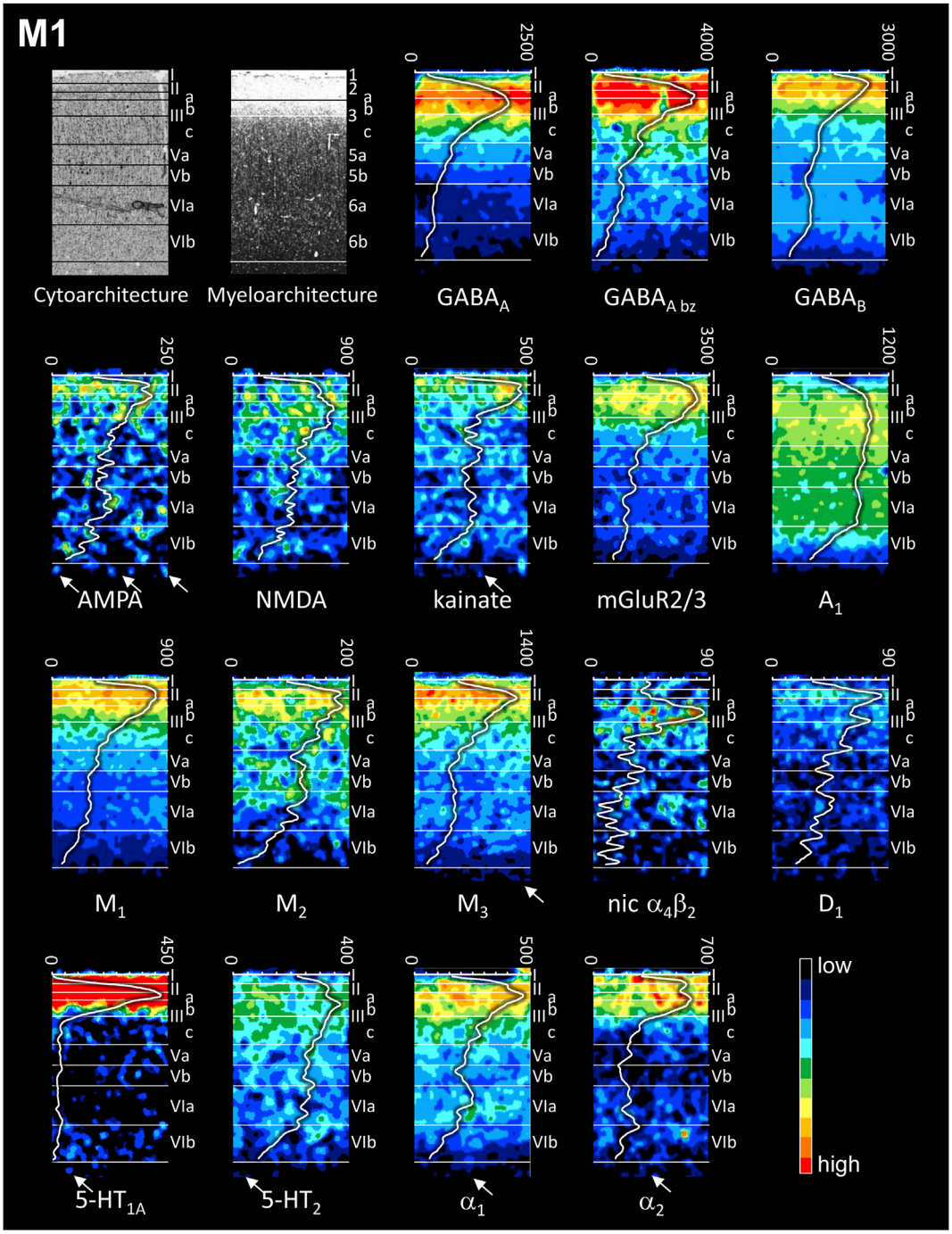

Fig. 5. Receptor-, cyto-, and myeloarchitecture of the human primary motor cortex (M1, BA4). The absolute receptor concentration (in fmol/mg protein) throughout the cortical depth is provided by the profile curve overlaid onto each receptor autoradiograph. Note, that the scale has been optimized for each profile to provide the best visualization of changes in receptor densities throughout the cortical ribbon. The myelin stained section shows less details and fewer fibers than shown in Fig. 4. This is due to the fact that the current section was obtained from deep-frozen, unfixed tissue, and no differentiation of the staining was performed. Roman and Arabic numerals indicate cyto- and myeloarchitectonic layers, respectively. Positions of cytoarchitectonic layers were transferred to the neighboring receptor images.

receptor densities are highest in c-layer IIIb and decrease gradually when moving towards c-layers I or VI. The A_1 receptors present the least distinctive distribution pattern of all examined receptor types, with a flat maximum spanning c-layers II–IV, only slightly lower densities in layers I and VI and lowest concentrations in layer VIb (Fig. 6). Notably, A_1 receptors are visible with low density in the white matter immediately below c-layer VIb.

Kainate and nicotinic $\alpha_4\beta_2$ receptors constitute notable exceptions due to their bimodal laminar patterns (Fig. 6). Kainate receptors show a superficial maximum in c-layer II and a second considerably lower one in c-layers V–VI. Nicotinic $\alpha_4\beta_2$ receptors reach a conspicuous maximum in c-layer IV and a lower second maximum in c-layer I. Interestingly, the nicotinic $\alpha_4\beta_2$ receptors are visible at higher concentrations in the white matter below the cortical ribbon than in c-layer VIb (see profile curve in Fig. 6).

3.3. Primary visual cortex (V1)

The primary visual cortex V1 is slightly thicker than the primary somatosensory cortex (2.5–2.9 mm, shrinkage corrected; Zilles and

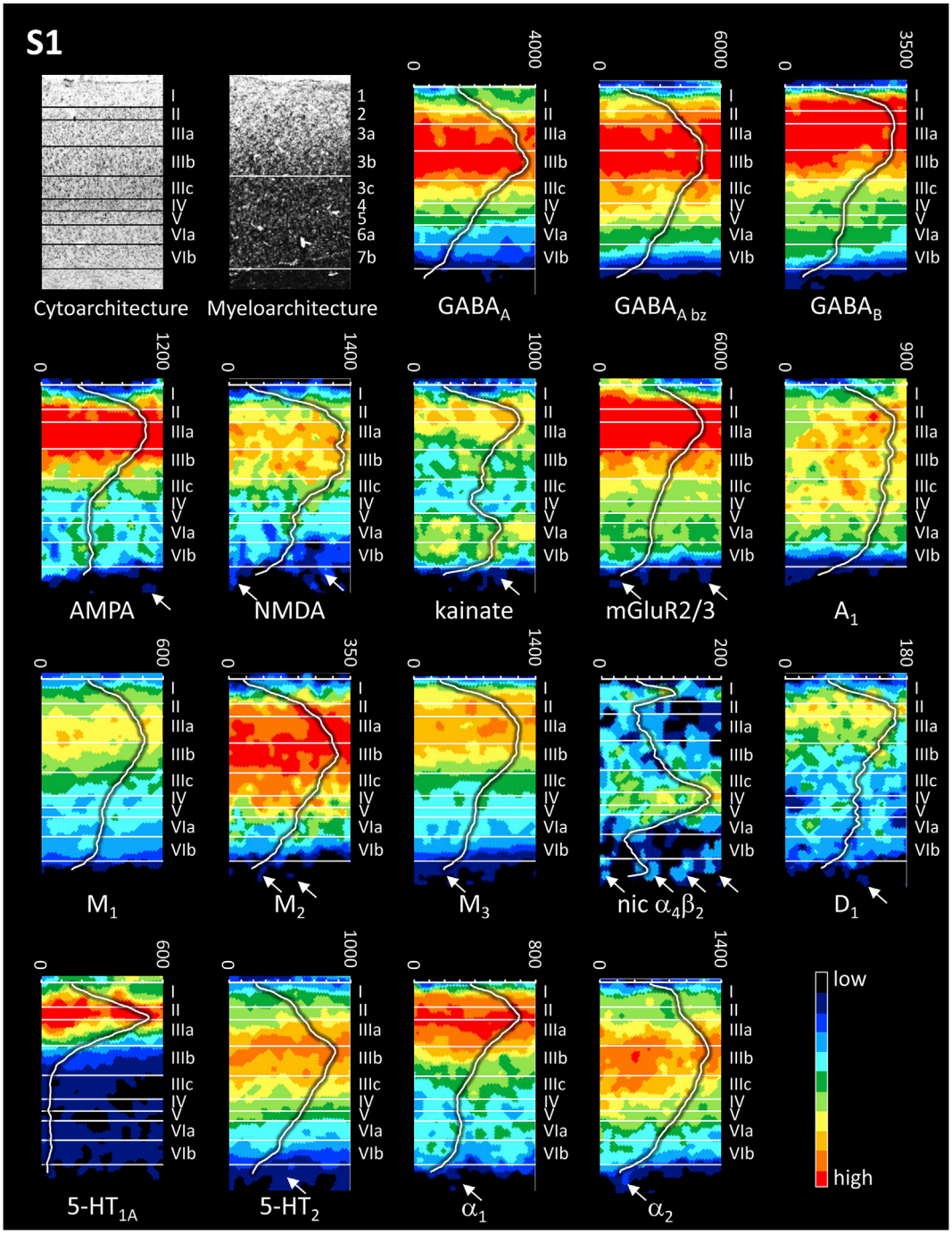

Fig. 6. Receptor-, cyto-, and myeloarchitecture of the human primary somatosensory cortex (S1, area 3b). For further details see Fig. 5.

Amunts, 2015). It is characterized by a prominent inner granular layer, which can be subdivided into four sublayers: IVa (superficial internal granular layer), IVb (intermediate internal granular layer corresponding to the Gennari stripe), IVcα and IVcβ (superficial and deep parts of the deep internal granular layer; Fig. 4). c-layer IVc reaches the highest, c-layer IVb the lowest cell packing density within the internal granular layer. Because of the koniocortical character of V1, all superficial layers are populated by small "granular" cells. The term "granular" cells is traditionally used in classic cytoarchitectonic descriptions for small more or less roundish appearing cells as seen in Nissl stained sections (Brodmann, 1909; von Economo and Koskinas, 1925). Immunohistochemical and electron microscopical observations have shown that these "granular" cells are in fact small pyramidal neurons, spiny and aspiny stellate cells, as well as other types of interneurons with a small-sized cell body. The koniocortical structure is typical of primary sensory areas, and characterized by a significant increase in the number and packing density of "granular" cells leading to a "*granularization*" (Sanides, 1962) of the upper cortical layers, resulting in a difficult delineation of layer II from layer III in Nissl stained sections.

In myelin-stained sections, the most conspicuous feature of V1 is a stripe of densely packed myelinated axons running parallel to the surface of the cerebral cortex. This m-layer 4b is found at the level of c-layer IVb, and constitutes the so-called stria of Gennari or outer Baillarger-stripe (Figs. 4 and 7). An inner Baillarger stripe (m-layer 5b) is also visible, but with a clearly lower density of myelinated fibers, at the level of c-layer Vb. As in M1 and S1, the vertical fiber bundles end at the border

between m-layers 3a and 3b.

The examined transmitter receptors show an intricate laminar distribution pattern in V1 (Fig. 7). Most receptors (with the notable exception of kainate, D_1, and 5-HT_{1A}) present a bimodal distribution pattern, though they differ in the width and location of the maxima relative to the c-layers. The kainate receptor has a trimodal distribution with maxima in c-layers I–II, IVa, and V–VI. Notable is a clearly higher density in c-layers V–VI than in the two superficial maxima. The D_1 receptor density is more or less equally distributed throughout all cortical layers of V1. The 5-HT_{1A} receptor density is clearly unimodal, with high concentrations in c-layers I to upper III followed by extremely low densities in all other layers. $GABA_A$, $GABA_{A\ bz}$, $GABA_B$, NMDA, A_1, M_1, M_2, M_3, and 5-HT_2 receptors reach their first maximum in layers II–IVa. The first maximum of AMPA, mGluR2/3, and α_1 receptors is restricted to c-layers II and upper III, whereas that of nicotinic $\alpha_4\beta_2$ receptors is in c-layers I–II, and that of α_2 only covers c-layer IVa. In case of the bimodally distributed receptors, a second maximum is found in c-layers IVc ($GABA_A$, $GABA_{A\ bz}$, nicotinic $\alpha_4\beta_2$, 5-HT_2), IVc-V (NMDA), IVc-VIa (M_2), V ($GABA_B$, M_3, α_1), V–VI (A_1, M_1, α_1), or VI (AMPA, mGluR2/3). The similarity in the distribution pattern of receptor densities of $GABA_A$ and 5-HT_2 receptors is remarkable. This may suggest a co-localization of both receptors at the laminar level. Equally remarkable is the similarity in the laminar distribution of AMPA and A_1 receptors. In summary, the highly differentiated cytoarchitecture of V1 is mirrored by very distinct

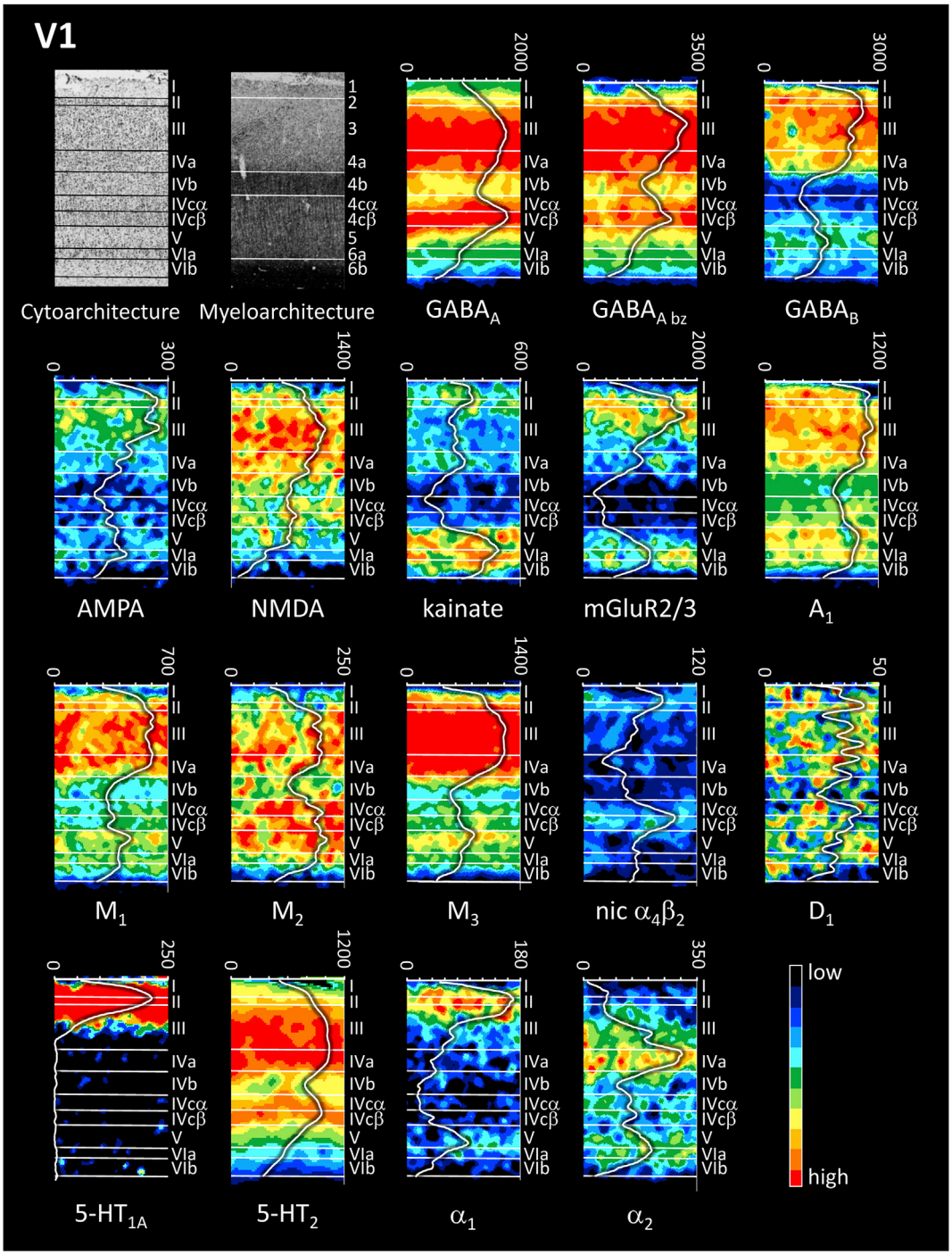

Fig. 7. Receptor-, cyto-, and myeloarchitecture of the human primary visual cortex (V1, BA17). For further details see Fig. 5.

distribution patterns of the different receptors.

3.4. Secondary visual cortex (V2)

The cortical thickness of V2 is 2.0–3.4 mm (shrinkage corrected; Zilles and Amunts, 2015). The cytoarchitecture of this higher unimodal sensory area is that of the typical isocortex, with cell dense c-layers II and IV, increased size of pyramidal cells in IIIc, and a relatively cell-sparse Va (Fig. 4). Layer I thickness is greater in V2 than in V1. The inner granular layer, which contains densely packed relatively large granule cells, and can be clearly demarcated from adjacent layers, does not show a differentiation into sublayers. The myeloarchitecture of V2 shows a much more prominent inner than outer Baillarger stripe, and a Kaes stripe (see Fig. 3) in m-layer 3a (Fig. 4). Densely packed vertical fiber bundles ascend to the 3a/3b border. The most conspicuous cyto- and myeloarchitectonical changes occur at the border between V1 and V2. V2 does not have a stripe of Gennari (Fig. 8).

Most of the receptors show a unimodal distribution in V2, with highest concentrations in the supragranular layers, although they differ in the sharpness of the maximum (reflecting abrupt or gradual changes in receptor densities), and/or in the cortical depth at which it is reached (Fig. 8). Nicotinic $\alpha_4\beta_2$ and 5-HT_{1A} receptors present narrow maxima, with highest densities in c-layers I and I–IIIa, respectively, followed by strikingly lower densities in the remaining layers. $GABA_A$, $GABA_{A\ bz}$,

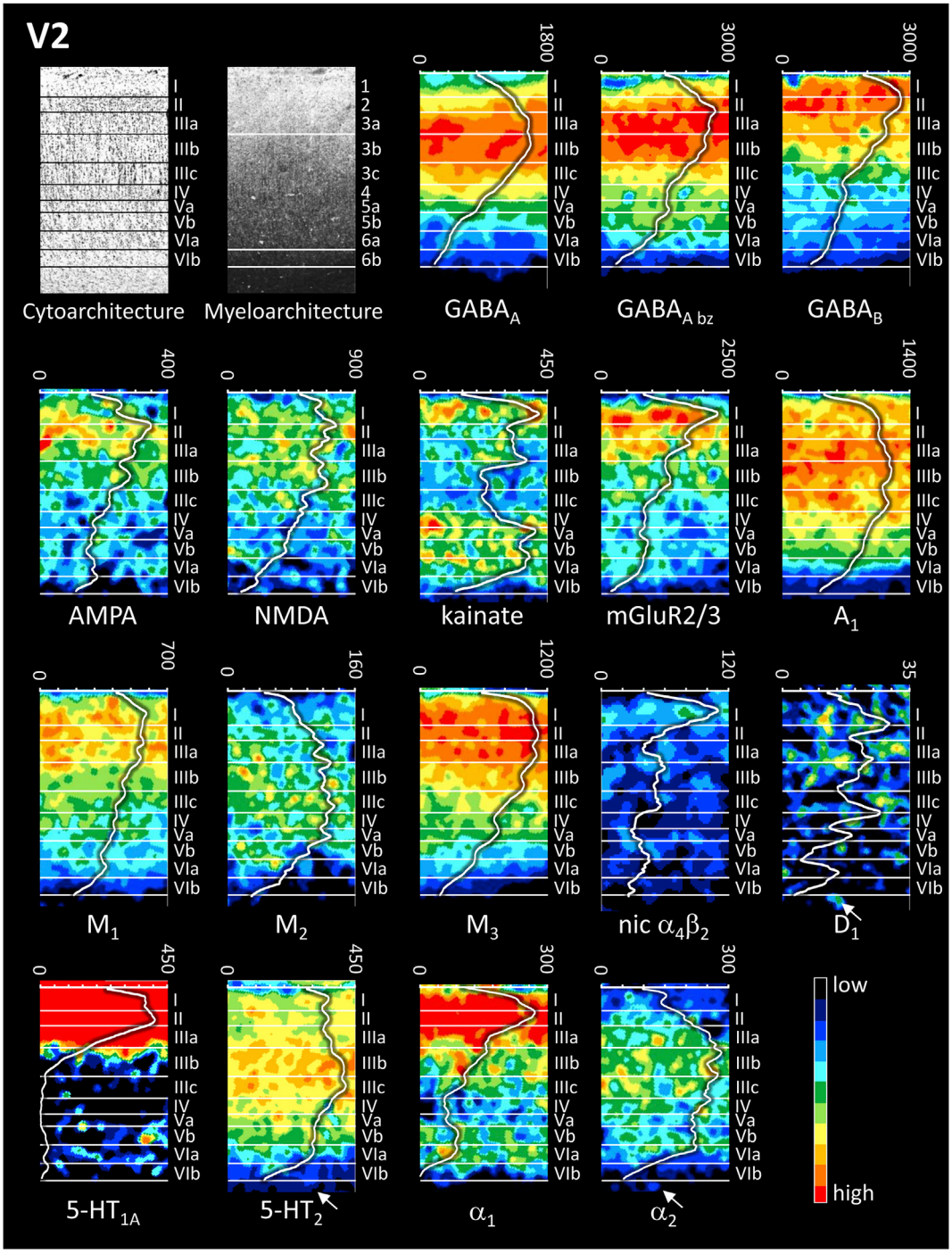

Fig. 8. Receptor-, cyto-, and myeloarchitecture of the human secondary visual cortex (V2, BA18). For further details see Fig. 5.

NMDA, and M_3 receptor densities increase gradually though c-layers I–II, reach maximum values in IIIa-IIIb, and decrease, again gradually, through IV–VI. The serotonin 5-HT_2 receptor differs only slightly from this laminar distribution pattern, since it reaches maximum values only in c-layers IIIb and IIIc, and the changes towards the pial surface or the cortical/white matter border are even more gradual. $GABA_B$ receptor densities are maximal in c-layer I; AMPA and M_1 in II–IIIa and I–IIIa, respectively. Very high densities of A_1, M_3, and D_1 receptors are found in all supragranular layers. The M_2 receptor reaches relatively high densities throughout c-layers IIIa-Vb, whereas the α_2 receptors reach a maximum in c-layers III–IIIc. Kainate and, to a lesser degree, α_1 receptors are exceptional, since they present a bimodal laminar pattern. Kainate receptors reach highest densities in c-layers I and IV–VIa. Lowest concentrations are found in c-layers IIIb and IIIc. Adrenergic α_1 receptors present a superficial maximum over c-layers I–IIIa separated from the second, considerably lower maximum in Vb-VIa. The profile curves of receptor densities are remarkably similar for the mGluR2/3 and α_1 receptors by their restricted localization of a first maximum in c-Layers I–IIIa and a second, much smaller maximum in Vb–VIa.

3.5. Area 44v

We studied here a part of BA44, i.e., area 44v (Amunts et al., 2010). The cortical thickness of BA44 is 3.0–3.9 mm (shrinkage corrected; Zilles and Amunts, 2015), and the thickness of 44v does not differ from that of BA44. The cytoarchitecture of this multimodal association area has a typical isocortical appearance, with a cell dense c-layer II and conspicuously large pyramidal cells in IIIc (Fig. 4). Pyramids in c-layer IIIa/b are

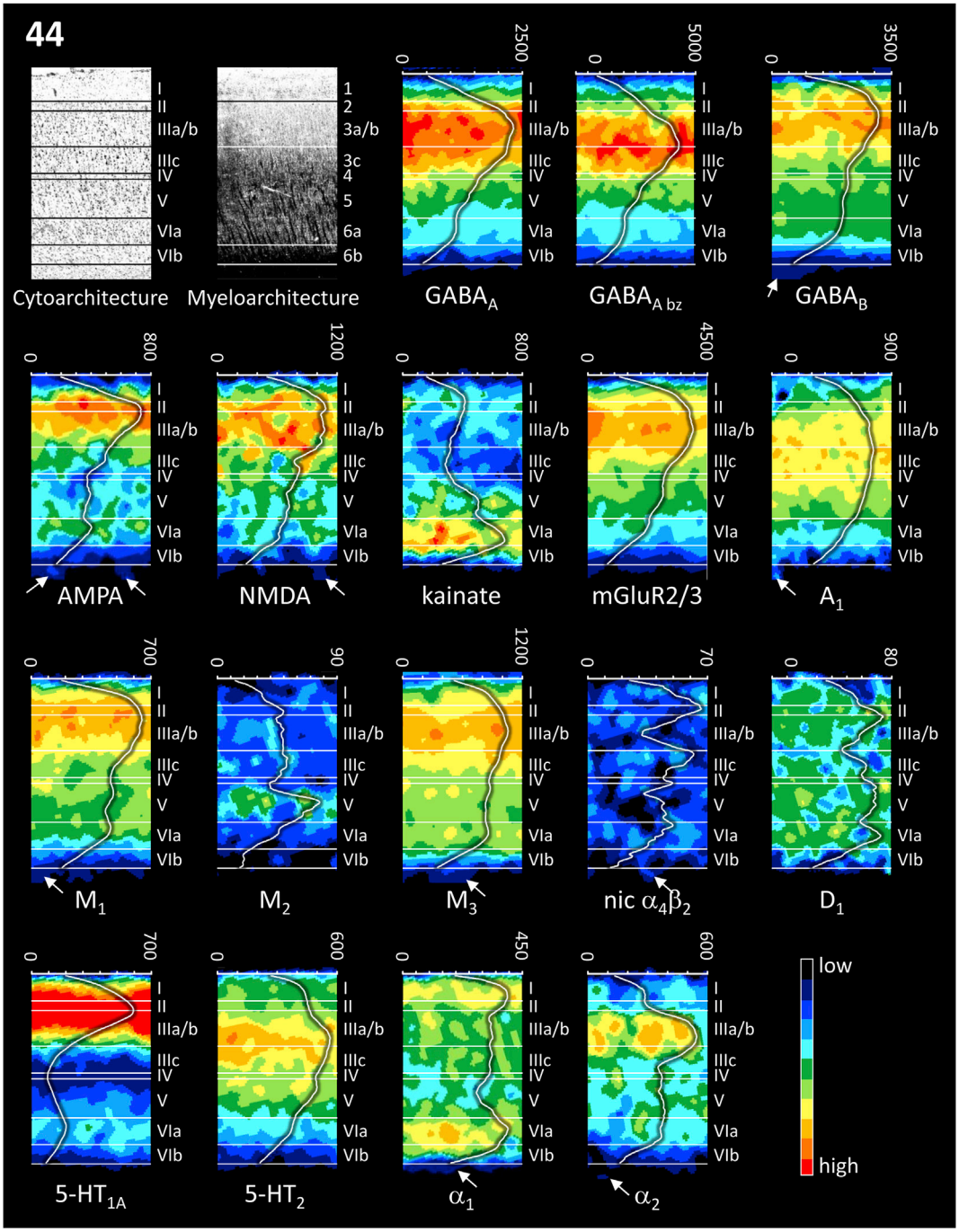

Fig. 9. Receptor-, cyto-, and myeloarchitecture of area 44 of the Broca region. For further details see Fig. 5.

considerably smaller than those in IIIc. Layer IV is thin and poorly developed. Therefore, the cytoarchitecture of this cortical area can be characterized as dysgranular. Layers Va and Vb can be clearly delineated from each other by the large pyramids in the former. The myeloarchitecture of BA44 shows a more prominent inner than outer Baillarger stripe (Fig. 4). Densely packed vertical fiber bundles are relatively long and reach into the lower part of m-layer 3a.

Most receptors in 44v show a unimodal distribution, but the extent and localization of the absolute maxima differ between the different receptors (Fig. 9). Whereas the $GABA_A$, $GABA_{A\ bz}$, $GABA_B$, AMPA, NMDA, mGluR2/3, M_1, and M_3 receptors display their maximal densities in supragranular c-layers I–IIIb/c, highest A_1 and 5-HT_2 densities are found in IIIb-IIIc, and the α_2 receptors reach maximal concentrations in c-layers IIIa-IIIb followed by a plateau from IIIc to the lower border of VIa. Thus, α_2 receptors seem to be concentrated in layers relevant for the prevailing cortico-cortical input. A very distinct and restricted distribution of relatively high concentrations of M_2 receptors is visible in layer V, although this receptor type shows a low absolute concentration in 44v. A bimodal distribution is found for the kainate, 5-HT_{1A} and α_1 receptors, with highest values in c-layers VIa (kainate and α_1), and in I–IIIa (5-HT_{1A}). The nicotinic $\alpha_4\beta_2$ and the dopaminergic D_1 receptors are more or less equally distributed throughout the cortex if their absolute low densities are taken into consideration.

3.6. Superior parietal cortical area 7A

We studied area 7A as a representative of BA7 in the superior parietal lobule. Its cortical thickness is between 2.6 and 4.4 mm (shrinkage

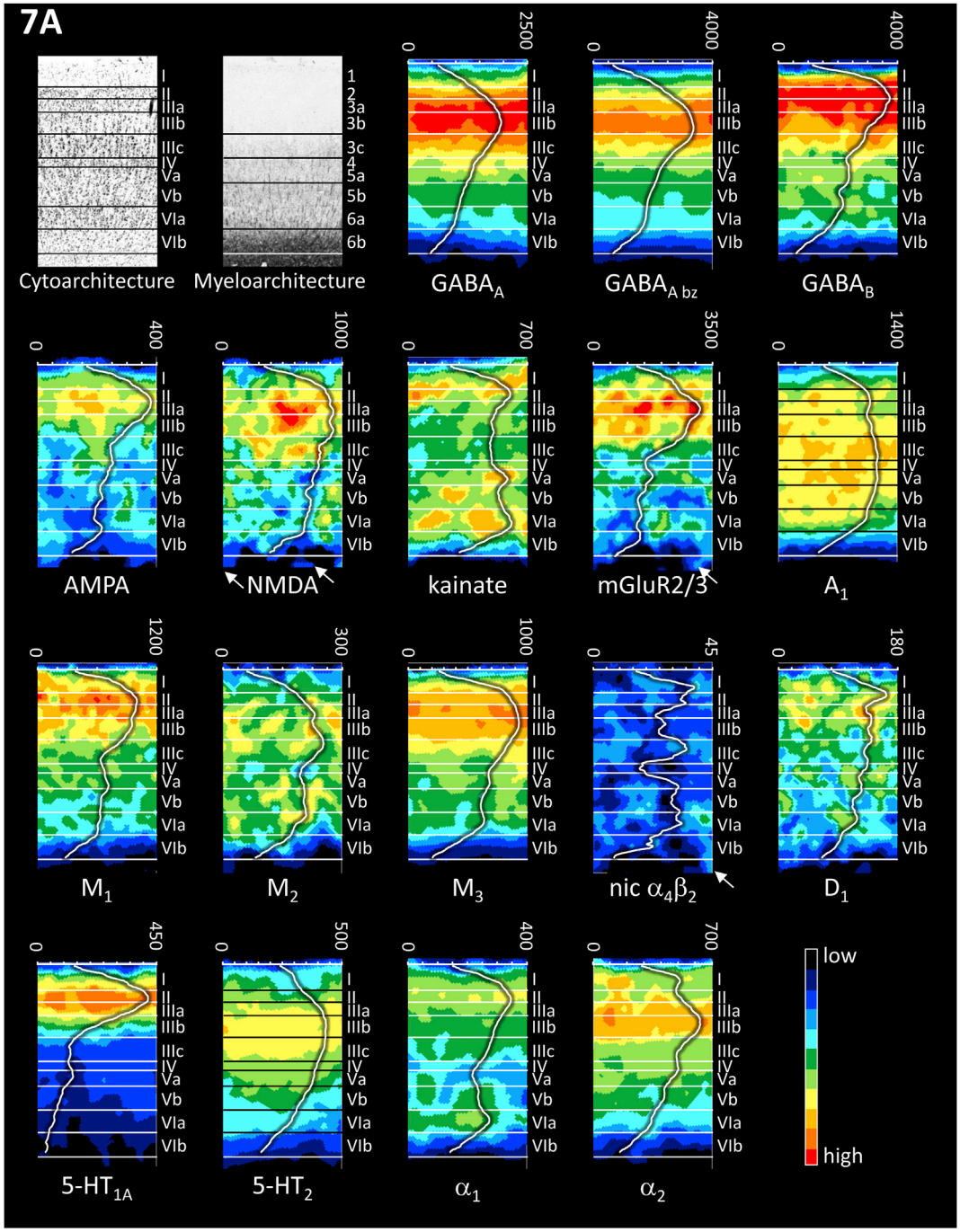

Fig. 10. Receptor-, cyto-, and myeloarchitecture of area 7A of the superior parietal lobule. For further details see Fig. 5.

corrected) depending on the curvature of the cortical ribbon. The cytoarchitecture of this isocortical multimodal association area is characterized by a diffuse border between c-layers II and IIIa, a low cell density in IIIb, and the presence of large pyramidal cells in IIIc. Layer IV is visible as a pale stripe between IIIc and Va, because the small granular cells have a small cytoplasmic rim around the clear nucleus in the cell body stain used in the present observation. A cell dense c-layer Va can be delineated from the cell sparse Vb. The same holds true for c-layers VIa and VIb (Fig. 4). The myeloarchitecture of 7A shows equally prominent inner and outer Baillarger stripes (Fig. 4).

As in 44v, most receptors in area 7A have a unimodal distribution of their laminar concentrations, with higher densities in the supragranular than in the infragranular layers (Fig. 10). Only the A_1 receptors reach a relatively high density throughout c-layers IIIc-Va. $GABA_A$, $GABA_{A\ bz}$,

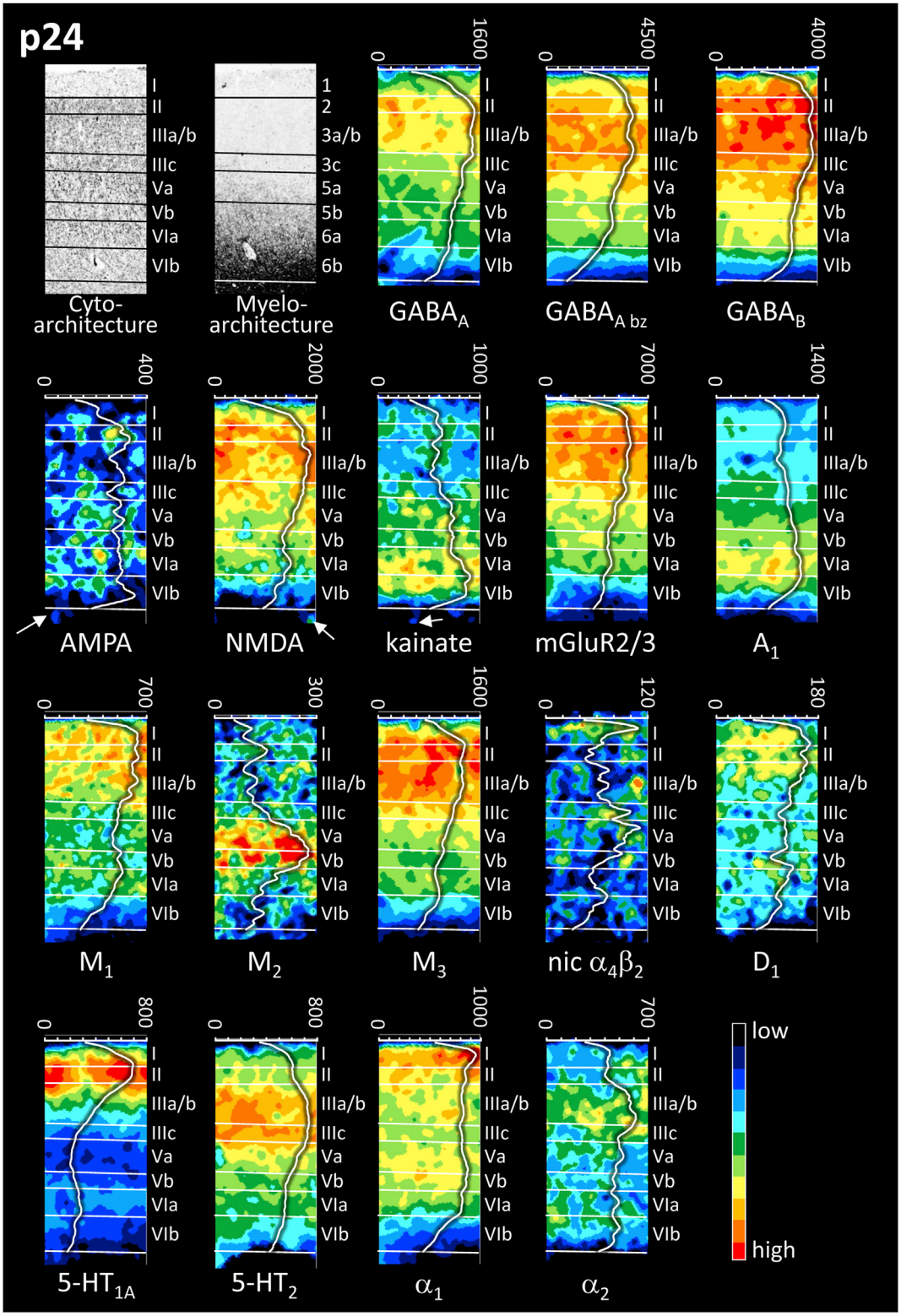

Fig. 11. Receptor-, cyto-, and myeloarchitecture of area p24 of the cingulate gyrus. For further details see Fig. 5.

NMDA, M_3, and α_2 receptor binding sites reach maximum densities in c-layers IIIa/b, and decrease gradually through layers IIIc to VIb. The 5-HT_2 receptors present a similar laminar pattern, but maximum values are found in IIIa-IIIc. Highest $GABA_B$, AMPA, and mGluR2/3 receptor densities are found closer to the pial surface, namely in c-layers I–IIIb ($GABA_B$), II–IIIa (AMPA) or II–IIIb (mGluR2/3). The laminar distributions of M_1, D_1, and 5-HT_{1A} receptors are almost restricted to c-layers II–IIIa. Kainate, M_2, and α_1 receptors present a bimodal density distribution. Kainate receptors reach two maxima of comparable height, one in c-layers I–II, the second in Va-VIa, separated by low concentrations in c-layer IIIc. The M_2 receptor is expressed at somewhat higher concentrations in c-layers II–III than in V–VIa. The α_1 receptor reaches a first maximum in c-layer II and a second, much lower one in VIa. Finally, the nicotinic $\alpha_4\beta_2$ receptors show a relatively equal distribution throughout all layers if their low absolute concentrations are taken into account.

3.7. Cingulate area p24

Periarchicortical area p24 is studied here as a representative of BA24. Its cortical thickness amounts to 3.0–3.5 mm (shrinkage corrected; Zilles and Amunts, 2015). Area p24 is agranular, i.e., lacks the inner granular c-layer IV. It is also characterized by a prominent c-layer V, which can be subdivided into Va with numerous densely packed large pyramids and a cell sparse Vb which stands out as a pale stripe due to the more cell dense c-layer VIa (Fig. 4). The myeloarchitecture of BA24 shows a very broad m-layer 1, an m-layer 4 which is hardly delineable from 5a, and a clearly visible inner Baillarger stripe in m-layer 5b. Most vertical fiber bundles are no longer visible above m-layer 4 (Fig. 4).

AMPA receptors are homogeneously distributed throughout c-layers II–VI. Many of the other receptors ($GABA_A$, $GABA_{A\ bz}$, $GABA_B$, NMDA, mGluR2/3, M_1, M_3, D_1, α_1) show a declining density from c-layers I or II to the border between VIa and VIb (Fig. 11). Maximal values are reached in these supragranular layers with the notable exception of kainate, A_1, and M_2 receptors, which reach their maximal density in c-layers VIa-VIb (kainate, A_1) or Va-Vb (M_2). The nicotinic $\alpha_4\beta_2$ receptor has local maxima in c-layers I and IIIc-Va, with minima in c-layers II and VIa. The sharpest inter-laminar differences are found for the 5-HT_{1A} receptor, which maximum in c-layers I and II is followed by very low densities in Va-VIb interrupted by a somewhat higher, but absolutely low density in VIa. Serotonin 5-HT_2 and adrenergic α_2 receptors also present relatively restricted maxima, which are located within c-layers IIIa-IIIc and IIIa/b, respectively.

3.8. Entorhinal cortex

The cytoarchitecture of the entorhinal cortex is completely different from that of the isocortex and of area p24. Moreover, the entorhinal cortex has been subdivided into several subareas by their cyto- and myeloarchitecture (Sgonina, 1937). As representative for the entorhinal cortex, we have analyzed subarea λ15, which is probably the equivalent of area Hʌ of von Economo and Koskinas (1925). The thickness of the cortical ribbon at this position is approximately 3 mm (shrinkage corrected). The difference between isocortex and the allocortical entorhinal area has already been highlighted by a different nomenclature (Sgonina, 1937), which is also used in the present study. c-Layer 1 is narrow and sparsely populated (Fig. 4). It is followed by a c-layer with flat cell islands called Preα. These islands cannot be recognized in all subareas of the entorhinal cortex. Below this layer, round islands of high cell density interrupted by nearly cell-free clefts build c-layer Preβ. The following layers Preγ_1, Preγ_2, and Preδ are delineable by somewhat increased (Preγ_1, Preδ) and decreased (Preγ_2) cell packing densities. Most characteristic for all entorhinal subdivisions, is c-layer Disa, with a very low cell packing density. Below Disa, c-layers Disb (high packing density of large pyramidal cells), Priα (lower cell density than in Disb), and Priβ (very low cell density) can be delineated.

Myelin stained sections reveal three m-layers with a very high (m-layer1 and Disa) to moderate (Priα) density of horizontally running fibers (Fig. 4). The vertical fiber bundles are exceptionally long and reach the border between m-layer 1 and Preα. The myelin-dense layers may be comparable by their position to the Cajal-Retzius stripe in m-layer 1, the outer Baillarger stripe in Disa, and the inner Baillarger stripe in Priα. However, the cytoarchitecture of Disa differs by the presence of pyramidal cells from that of the isocortical inner granular layer (c-layer IV), in which the outer Baillarger stripe of the isocortex is found. This finding underlines a principal difference between the isocortical lamination pattern and that of the entorhinal cortex.

The receptor architecture of the entorhinal cortex differs considerably from that of isocortical areas. Some receptors ($GABA_B$, AMPA, mGluR2/3, M_1, M_3, α_1, and α_2) reach highest densities in the superficial half of the entorhinal cortex (Fig. 12). The $GABA_A$, $GABA_{A\ bz}$, and adenosine A_1 receptors show highest densities in Preγ_2, whereas the highest concentrations of M_2 and nicotinic $\alpha_4\beta_2$ receptors are found in Preδ. Similarly restricted is the highest 5-HT_{1A} receptor density, but it is located in c-layer Preβ. The NMDA receptors show a patchy distribution of high and low concentrations throughout all cortical layers. The kainate receptor is most densely packed in c-layer Priα and the upper part of Priβ followed by a medium density in Preα and Preβ. Lowest densities of this receptor are found in c-layer 1 and the lower part of Preβ near to the cortex/white matter transition. The 5-HT_2 receptor is equally dense through all cortical layers except c-layers 1 and Priβ, where the lowest concentrations are found. The D_1 receptor gradually increases from c-layer 1 to the border between Priα and Priβ.

Since the islands in Preβ are most conspicuous in cytoarchitecture (area labeled by asterisks in the cytoarchitectonic image of Fig. 12), we located the center of such islands in the neighboring receptor autoradiographic images of the same brain. Their position is indicated by asterisks. Most notable is the perfect match of highest 5-HT_{1A}, as well as low α_2 and M_2 receptor densities in the centers of such islands in c-layer Preβ. Since we used neighboring sections, and the size of the islands is too small to be found precisely at the same place in all sections, in some cases we could identify more or less centers of islands in the different receptors.

Figs. 13–16 show a comparison of the receptor profiles of all cortical areas studied here. We have arranged the absolute receptor densities (fmol/mg protein) throughout all cortical layers so that all GABA receptors and the mGluR2/3 receptor, which reach the highest densities, the ionotropic glutamate and the adenosine A_1 receptors, the serotonergic, adrenergic and muscarinic M_3 receptors, and the muscarinic M_1 and M_2, nicotinic $\alpha_4\beta_2$ and dopaminergic D_1 receptors are shown in separate plots because these four groups each reach considerably different absolute densities. The GABA receptors show higher densities in the primary sensory (S1, V1) than in the second sensory cortex (V2). By far the highest densities of mGluR2/3 receptors are found in the allocortical entorhinal and cingulate areas, and the lowest densities in the visual areas V1 and V2. The highest $GABA_A$ receptor density is found in S1, and the lowest in the allocortical regions p24 and entorhinal cortex, where the $GABA_B$ receptor reaches its highest densities. The highest AMPA and NMDA receptor densities are found in the entorhinal cortex and S1, respectively. The kainate receptor is most densely concentrated in the entorhinal cortex. Highest densities of the nicotinic $\alpha_4\beta_2$ receptor are reached in c-layers IIIc and IVc of S1 and V1, respectively. The motor cortex (M1) contains the highest density of muscarinic M_1 receptors, whereas the muscarinic M_2 receptor reaches highest values in the allocortical regions p24 and entorhinal area, as well as in the primary sensory cortices (S1 and V1). The maximal muscarinic M_3 receptor density is several times higher than that of the other muscarinic receptors in all areas studied here. D_1 receptors are most prominent in S1, area 7A, and the allocortical areas, but only reach overall relatively low absolute densities when compared to those of other neurotransmitter systems. The adrenergic and serotoninergic receptors show low densities averaged over all cortical layers, with the notable exception of 5-HT_2 receptors in the primary sensory areas. Finally, the exceptionally high density of 5-HT_{1A} and α_2 receptors in the allocortical areas is a major difference

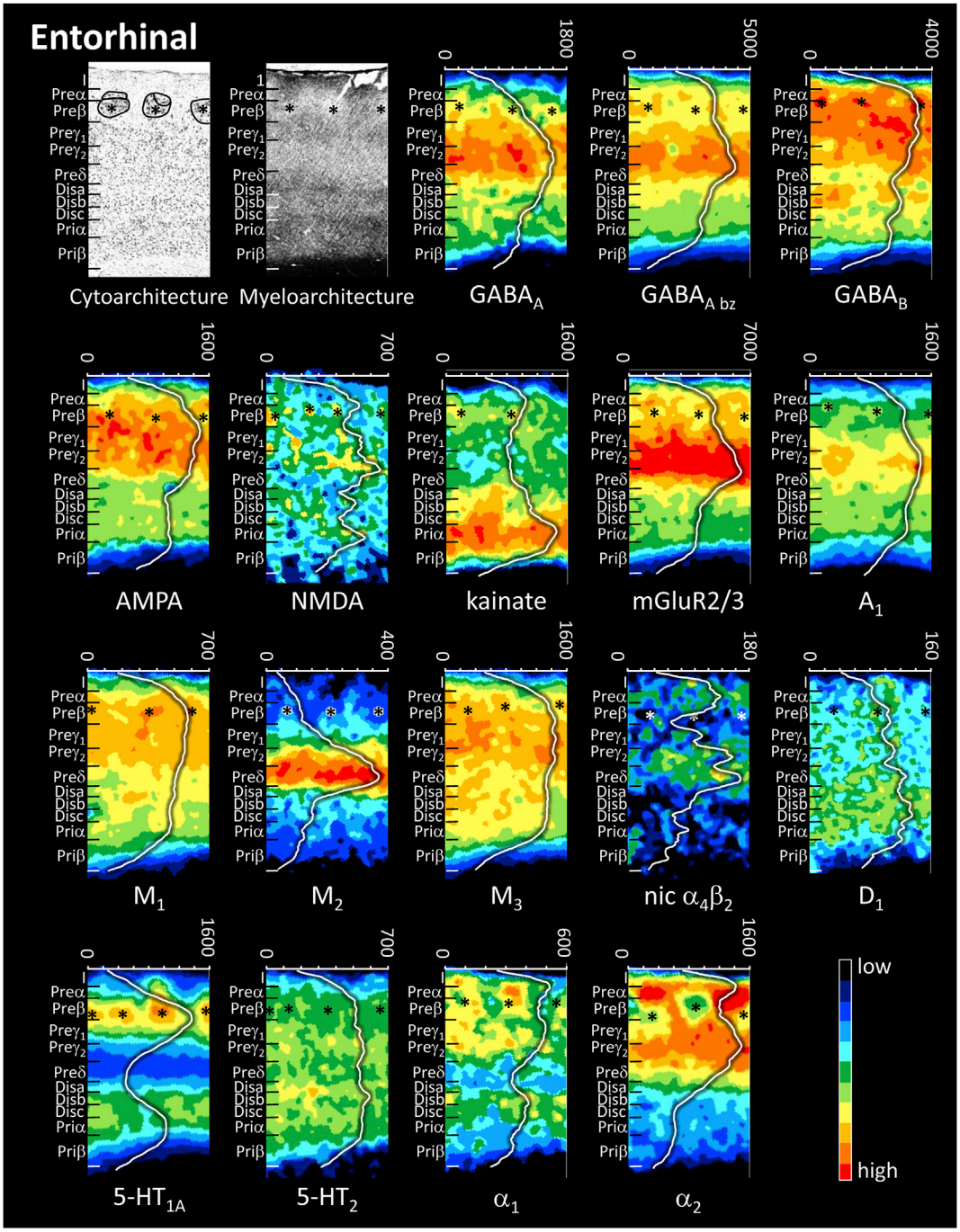

Fig. 12. Receptor-, cyto-, and myeloarchitecture of the entorhinal cortex. For further details see Fig. 5.

between those regions and the isocortex.

To provide an impression of the interindividual variability of the receptor profiles, we calculated for each lamina and receptor the mean receptor density over all examined areas except the entorhinal cortex, which has a laminar organization not comparable with that of all isocortical areas or that of cingulate area p24 (Fig. 17).

4. Discussion

The present observations provide a comparison of the nerve fiber and receptor distributions in layers of representative areas of the human cerebral cortex with classical cytoarchitectonic descriptions of their layering pattern (Brodmann, 1909; Vogt and Vogt, 1919; von Economo and Koskinas, 1925). In most publications, cortical layers were identified in Nissl (cell body) stained sections. Therefore, most authors correlate MR-data with the cytoarchitectonic parcellation of layers although high resolution magnetic resonance imaging is more sensitive to myelin than to cell bodies. However, the question remains whether the myelo- (m-layers) and cytoarchitectonic (c-layers) laminar parcellations differ or coincide. Receptor autoradiography visualizes radioligand binding to sites in the receptor molecular structures, which are by far more frequently located on dendrites than on cell bodies. Therefore, the laminar distribution patterns of neurotransmitter receptors (r-layers) was studied, and the r-layers of 17 receptors were compared with c-layers in neighboring cell body stained sections of the same brains. Since cortical areas differ in their c- and m-layer patterns, regional differences of these laminations between cortical areas must be taken into account. Therefore, we analyzed the c-, m- and r-layers of eight cortical areas of which

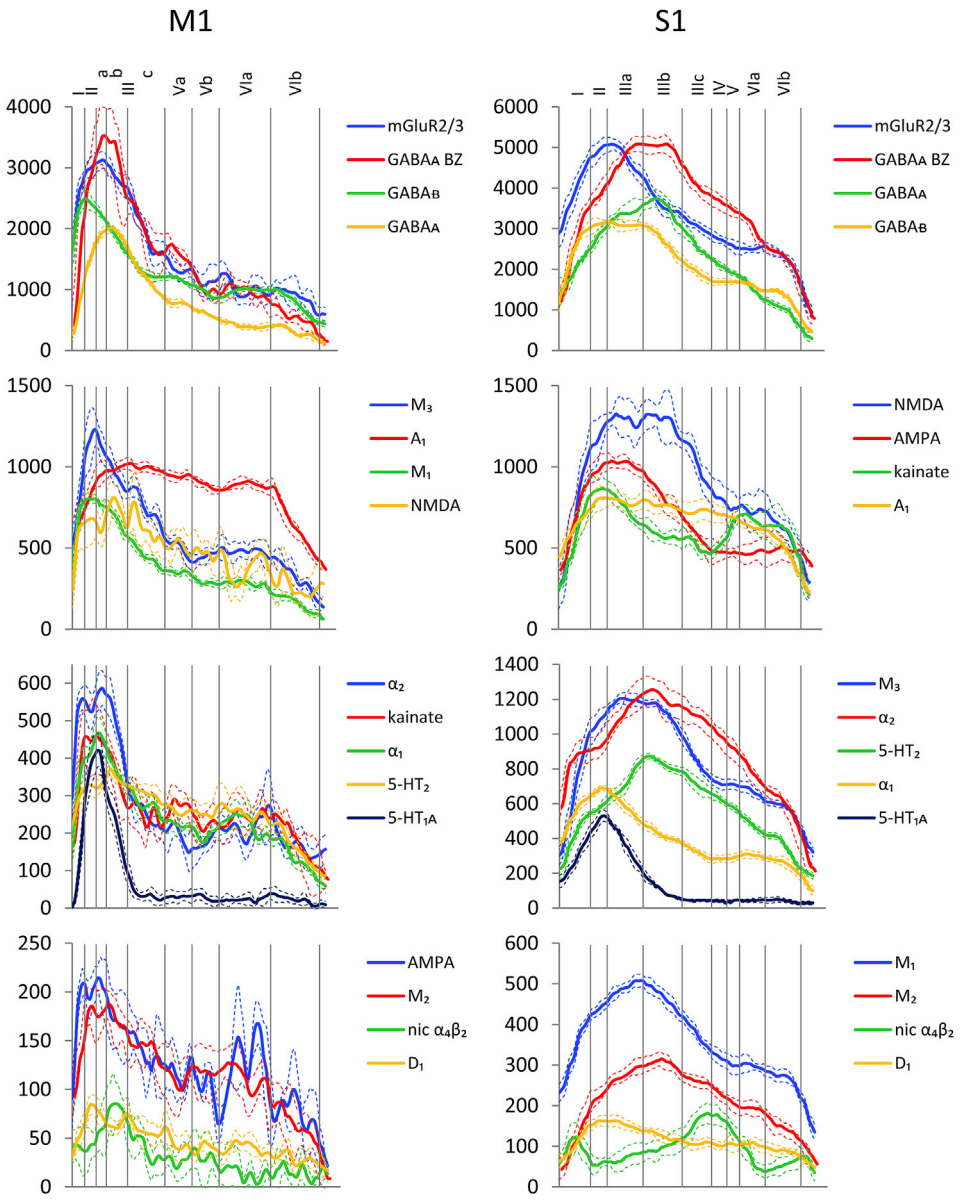

Fig. 13. Laminar receptor profiles in the primary motor (M1) and somatosensory (S1) cortices. Receptor densities (y axis) are given in fmol/mg protein. Roman numerals code for c-layers. Since the different receptor types occur at highly differing absolute densities in cortical areas and layers, the receptors are presented in four different groups with each showing a different scaling of the y axis.

six have been classified as isocortical, and two as allocortical (Brodmann, 1909; Sanides, 1964; Sgonina, 1937; Stephan, 1975; Vogt and Vogt, 1919). As representative areas of the isocortex, we selected the primary motor cortex M1, because this area does not have a clearly recognizable layer IV (Brodmann, 1909; von Economo and Koskinas, 1925), although the typical "granular" cells of layer IV have been demonstrated (Barbas and Garcia-Cabezas, 2015; Garcia-Cabezas and Barbas, 2014), the primary somatosensory cortex S1, and the primary visual cortex V1 as examples of typically unimodal sensory areas with a well-developed inner granular layer IV and an invasion of the more superficial layers by numerous small spiny stellate cells ("granular" cells in cell body stained sections; koniocortex). Furthermore, we analyzed the lamination of the secondary visual cortex V2 as an example of a higher unimodal sensory area, and that of areas 44 (Broca region) and 7A (superior parietal lobule) as examples of multimodal association cortices. Finally, we studied the lamination of area 24 (part of the cingulate gyrus) and of the entorhinal cortex (part of the parahippocampal gyrus) as representatives of the limbic cortex and the classical allocortex, respectively.

Cortical layers have classically been defined by differences in their prevailing cell types, packing density and sizes of cell bodies, or of myelinated fibers, as well as their connectivity patterns:

- c-layer I is populated by only a few scattered non-pyramidal neurons (Cajal-Retzius and spiny stellate cells), but mainly contains the terminal ramifications of apical dendrites of pyramidal neurons of deeper layers, and horizontally oriented axons from M-type thalamic neurons (Cajal-Retzius stripe in myeloarchitecture) (Jones, 1998; Rubio-Garrido et al., 2009; Shipp, 2007). Additionally, it receives input from the amygdala (Amaral and Price, 1984; Freese and Amaral, 2005) and from other cortical layers (e.g., Vogt and Pandya, 1978). The feedback projections from V2 to V1 terminate in layer I, but also in layers II, III, IVb, V and VI (Burkhalter and Bernardo, 1989).
- c-layer II comprises small pyramidal and interneurons. The apical dendrites of the pyramids reach c-layer I, and their axons extend into layer Vb, with numerous collaterals to all layers on their way from II to Vb. Layer II receives input from other isocortical regions.

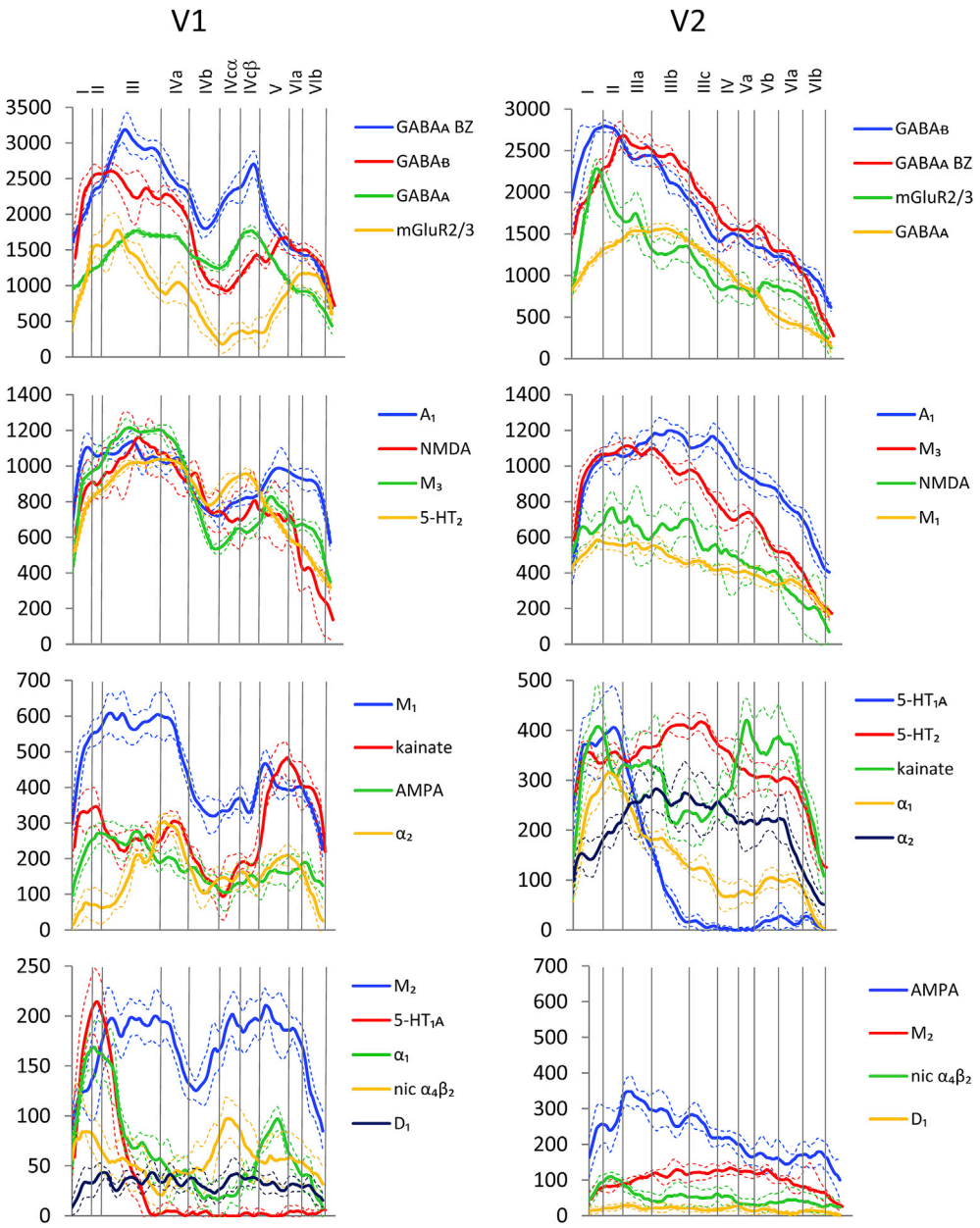

Fig. 14. Laminar receptor profiles in the primary (V1) and secondary (V2) visual cortices. For further details see Fig. 13.

- c-layer III, the main source for cortico-cortical connections, contains small and medium-sized pyramids, particularly in IIIa-b, and large pyramidal cells in sublayer IIIc of many higher-order associative areas. The subdivision into sublayers IIIa, b, and c is regionally distinct and not visible in all cortical areas. Numerous non-pyramidal neurons are also present in this layer. The dendrites of the pyramids extend up to layer I, and their vertically oriented intracortical axons extend with numerous collaterals to layers II to VI. Layer III projects to other hierarchically higher (from deeper layer III) and lower (from upper layer III) cortical areas, as well as to the striatum (Reiner et al., 2003; Wilson, 1987). Spreading of the fluorescent tracer DiI in human post mortem tissue blocks revealed that layer III pyramids are a major source and target of callosal projection fibers. Within human V1, the cytochrome oxidase blobs of layer III project to nearby blobs and avoid interblobs, whereas the interblobs project to nearby interblobs suggesting a functional parcellation within a cortical layer (Burkhalter and Bernardo, 1989). Tangential connections within and between auditory areas of the human cortex were also described. The primary auditory cortex is connected with surrounding belt areas through intracortical fibers and with thin but relatively long fiber tracts located between layer VI and the white matter (Tardif and Clarke, 2001), which probably represent U-fibers. Injections with biotinylated dextran amine in human post mortem tissue blocks containing Broca's region revealed horizontal connections within all layers. Most retrogradely labeled cell bodies were found in the supragranular layers. Thus, intrinsic connections show a strong laminar specificity within Broca's region (Tardif et al., 2007).
- c-layer IV is populated by spiny and aspiny stellate and pyramidal cells. It is particularly wide in the primary sensory areas, well visible in many areas of the isocortex, and hardly visible or completely lacking in motor and parts of the cingulate cortices. It is the main target of axons from thalamic C-type neurons, and receives numerous intra-hemispheric cortico-cortical afferents. The dendrites and axon collaterals of layer IV pyramids extend up to layer I (Mohan et al., 2015). The projections from human V1 to V2 terminate in layers III and IV of V2, those from V2 to V1 terminate in upper and lower layers

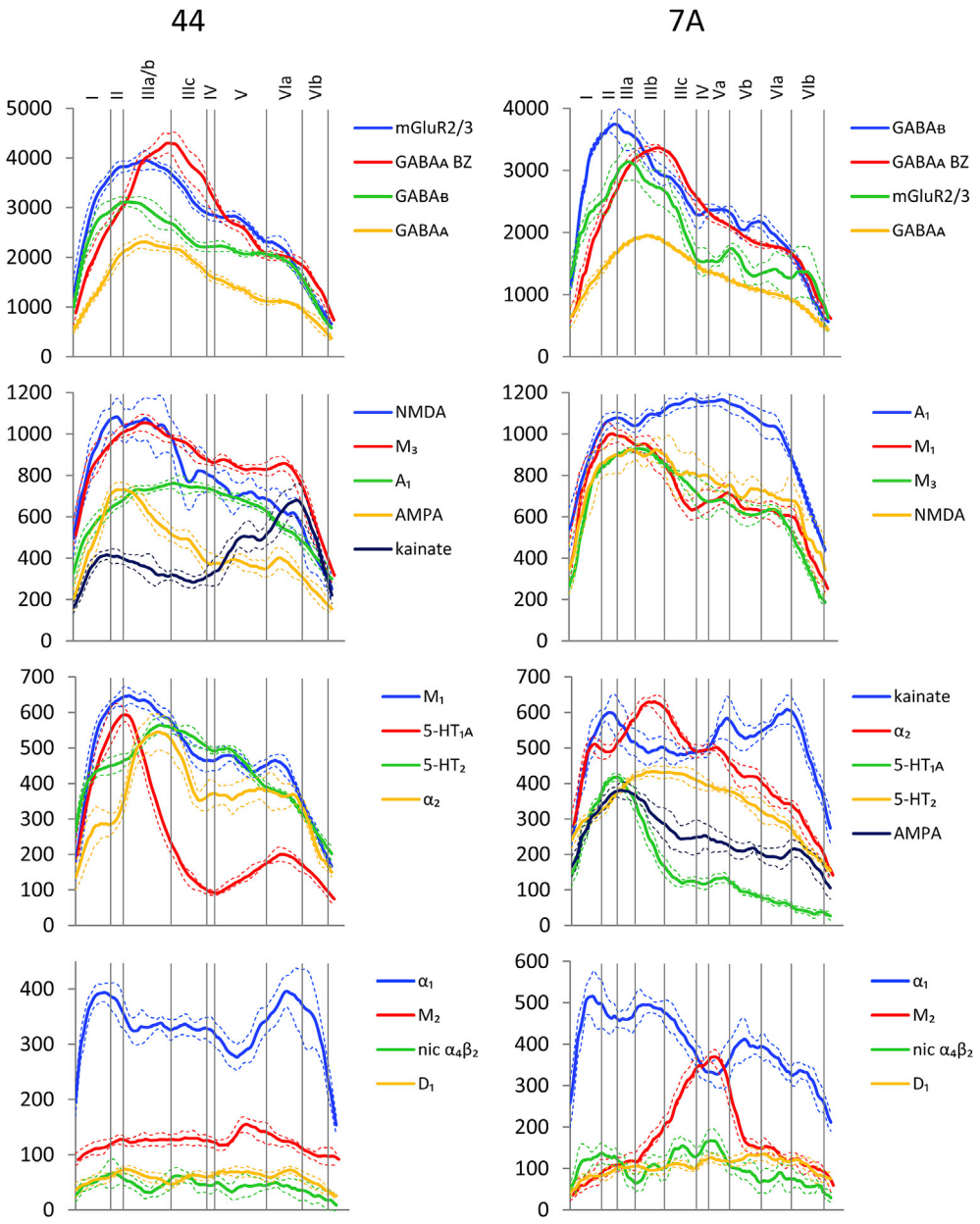

Fig. 15. Laminar receptor profiles in area 44 of the Broca region and of area 7A of the superior parietal lobule. For further details see Fig. 13.

(Burkhalter and Bernardo, 1989). Layer IV in the primary visual cortex is differentiated into sublayers IVa, IVb and IVc. Layer IVb, but not layers IVa or IVc, receives input from V2. This backward connection is probably part of the magnocellular stream (Burkhalter and Bernardo, 1989). The forward connections from V1 to V2 originate in layer IVb of V1 and terminate in the thick cytochrome oxidase stripes of V2, which are probably the source of the above mentioned feedback connections (Livingstone and Hubel, 1987).

- c-layer V mainly contains pyramidal neurons and can be subdivided into Va and Vb based on differences in the size and packing density of the neurons they contain. It projects into many subcortical regions including basal ganglia, thalamus, tectum, pons, and brain stem nuclei. The giant Betz cells of layer Vb in the primary motor cortex directly reach the spinal cord. Layer V of human V1 receives input from V2 (Burkhalter and Bernardo, 1989). Additionally, layer V is a source of ipsilateral cortico-cortical and callosal projections (Segraves and Rosenquist, 1982).
- c-layer VI can be subdivided into VIa (densely populated) and VIb (low neuronal density) and comprises a few large pyramidal neurons and many small spindle-like pyramidal and non-pyramidal neurons. Layer VI is reciprocally connected with the thalamus and sends efferent fibers to the other cortical areas. Additionally, input from the amygdala to c-layers V and VI is present (Freese and Amaral, 2005). The apical dendrites of layer VI pyramids reach the IIIa/IIIb border, with many oblique branches on their way.

4.1. *Comparability of c-, m- and r-layers*

The borders of c- and m-layers can be found at comparable positions in each of the various cortical areas studied here despite the completely different tissue compartments which are highlighted by cell body or myelin staining, respectively. m-layers characterized by an intermediate (Kaes stripe in m-layer 3a of V2) or extremely high to intermediate (outer

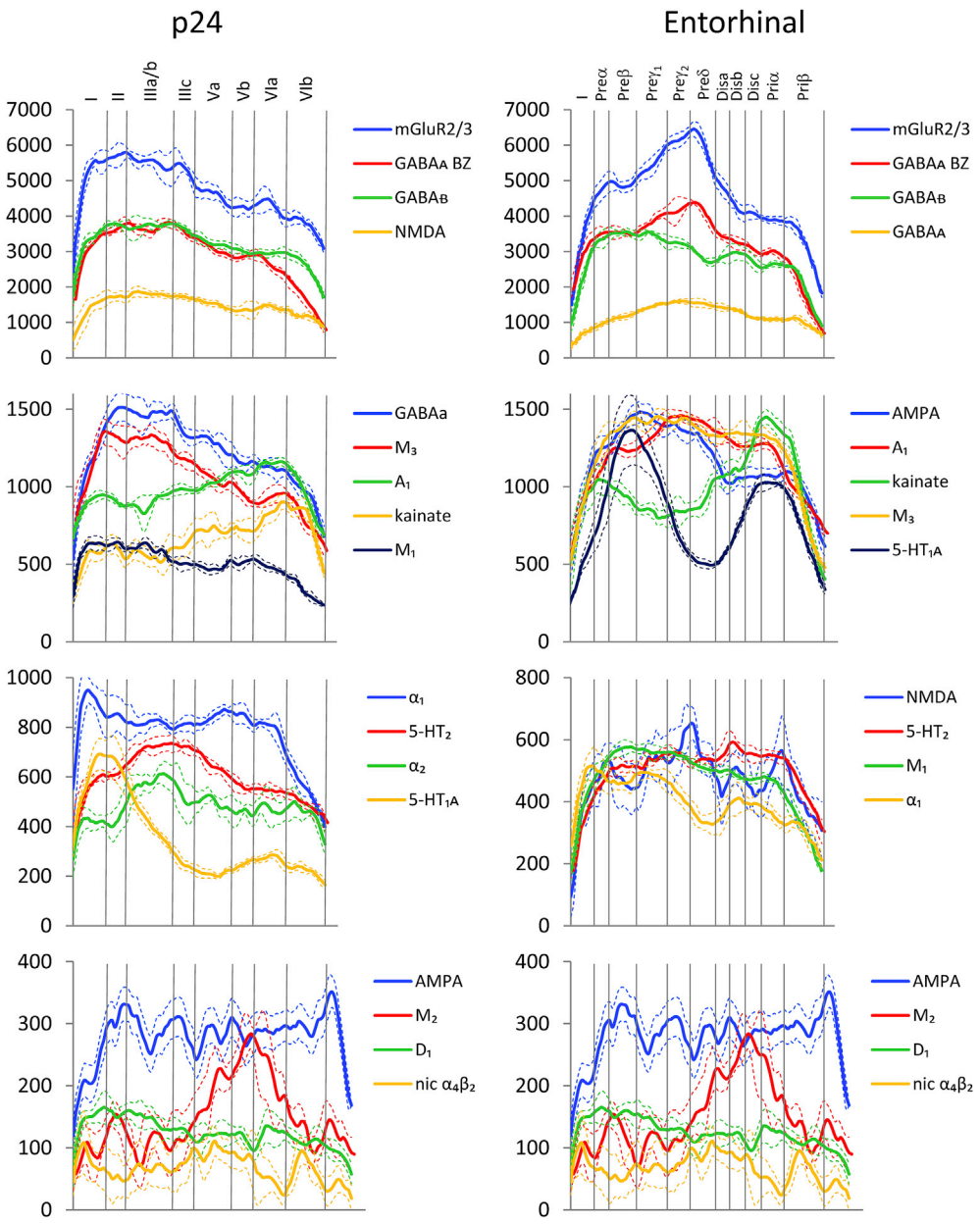

Fig. 16. Laminar receptor profiles in the cingulate area p24 and the posterior entorhinal cortex. For further details see Fig. 13.

stripe of Baillarger in m-layer 4 of V1, or areas 3b and 7A, respectively) density of horizontally running fibers are found adjacent to those devoid of or sparsely populated by such fibers. Only in m-layer 1 are further subdivisions visible, whereas c-layer I does not display a further subdivision of this layer.

At a first glance, the borders between c-layers may seem less sharp than those of m-layers. This is due to the fact that definitions of c-layers are based on various features, e.g., packing density of neuronal bodies, occurrence of various cell types, and differences in shapes and sizes of cell bodies (Zilles et al., 2002b). c-layers containing pyramidal-shaped neurons of different sizes (layers III and V) are interleaved with c-layers containing small ("granular") neurons (layers II and IV). Although the visibility of layer IV (granular, dysgranular, "agranular") and of the horizontal fiber stripes varies between the different cortical areas, comparable c- and m-layers can be defined in all isocortical regions. E.g., the horizontally running myelinated fibers which enable the delineation of isocortical m-layers 1, 4 and 5b are found at a position occupied by c-layers I (only a few scattered, small neuronal cell bodies), IV (densely packed small cells) and Vb. Layer Vb of the isocortex can be distinguished from Va by a higher packing density of pyramidal neurons and larger pyramidal cells in Vb.

In contrast to the borders of c- and m-layers, changes in receptor densities occur mainly in a gradual manner, resulting in blurred receptor profile curves (Figs. 5–16). As a consequence, the cortical ribbon presents a smaller number of r- than of c-layers. Furthermore, the width and localization of r-layers rarely coincide precisely with those of c-layers. This can be explained by the fact that the majority of receptors are located on the dendrites of cortical neurons, and not on their cell bodies (Alonso-Nanclares et al., 2008; Kooijmans et al., 2014; Sacco et al., 2009). Although a large number of the inhibitory GABA receptors are also found around the somata and the proximal axonal segment, the majority of GABA receptors and particularly all the other receptors, are indeed expressed on dendrites (Alonso-Nanclares et al., 2008; Megías et al., 2001; Merchan-Perez et al., 2014) Additionally, since the dendrites of pyramidal cells cross the borders of c- and m-layers (Mohan et al., 2015), it is important to keep in mind that, e.g., activation of receptors

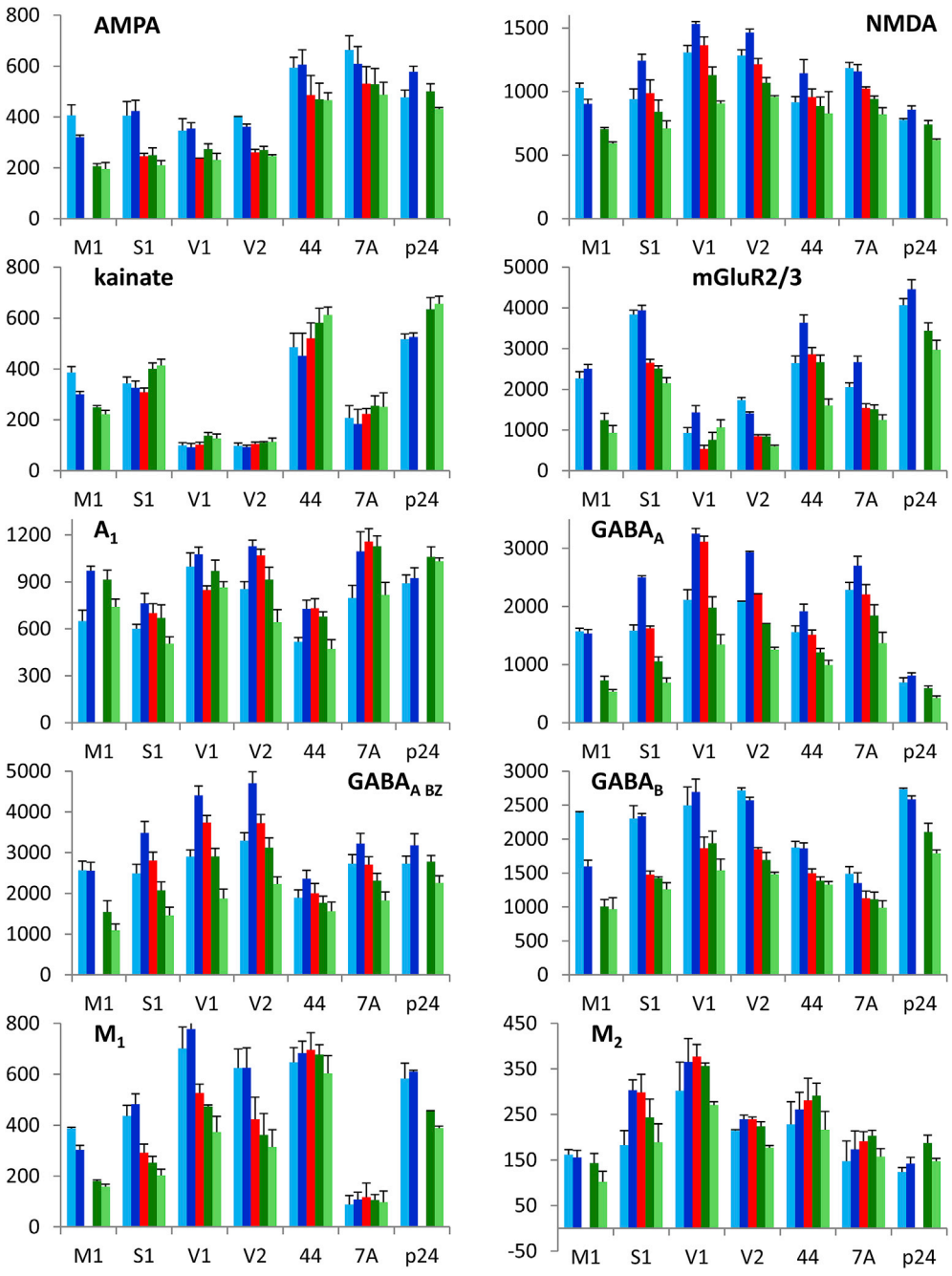

Fig. 17. Mean (+/-SE) laminar receptor densities averaged over all cases. Each receptor is separately shown because of the large differences in absolute receptor densities. X axis cortical area, y axis receptor density in fmol/mg protein.

located within c-layer III may result in an excitation, inhibition or modulation of pyramidal cells belonging to c-layers V.

A differential laminar degradation of the tissue may be an important methodical problem in studies of formalin or paraformaldehyde fixed brains, since the diffusion of the fixative takes a long time from outside to inside and may result in artifacts of staining intensity. Here, we report deep freezing of the brain in isopentane (Material and Methods), which leads to a complete freezing throughout the whole native brain in less than 5 min. It is impossible that an autolytic degradation occurs along the freezing gradient within this very short time. Moreover, we describe differences in laminar densities of receptors which are independently varying from a presumed general outside-inside-gradient. E.g., some receptors show high densities in the superficial layers, others show low densities in these layers compared to deeper layers. Also, a single receptor type may reach the same density in superficial and deep layers. Most importantly, we found the same receptor distribution patterns in deep frozen whole brains or large blocks of brains compared to deep frozen slices of 300–500 μm thickness which were sliced and deep frozen less than 15 min after surgical excision (Graebenitz et al., 2011; Palomero-Gallagher et al., 2012; Zilles et al., 1999). Particularly the last findings exclude the possible degradation effect.

4.2. *Regional specificities in receptorarchitecture*

Whereas the laminar distribution of some receptors remains constant throughout all isocortical areas (e.g., AMPA, NMDA, GABAergic, or M_3 receptors), other receptors present striking interareal differences. Kainate receptors show maximal densities in layer I of M1, but an additional

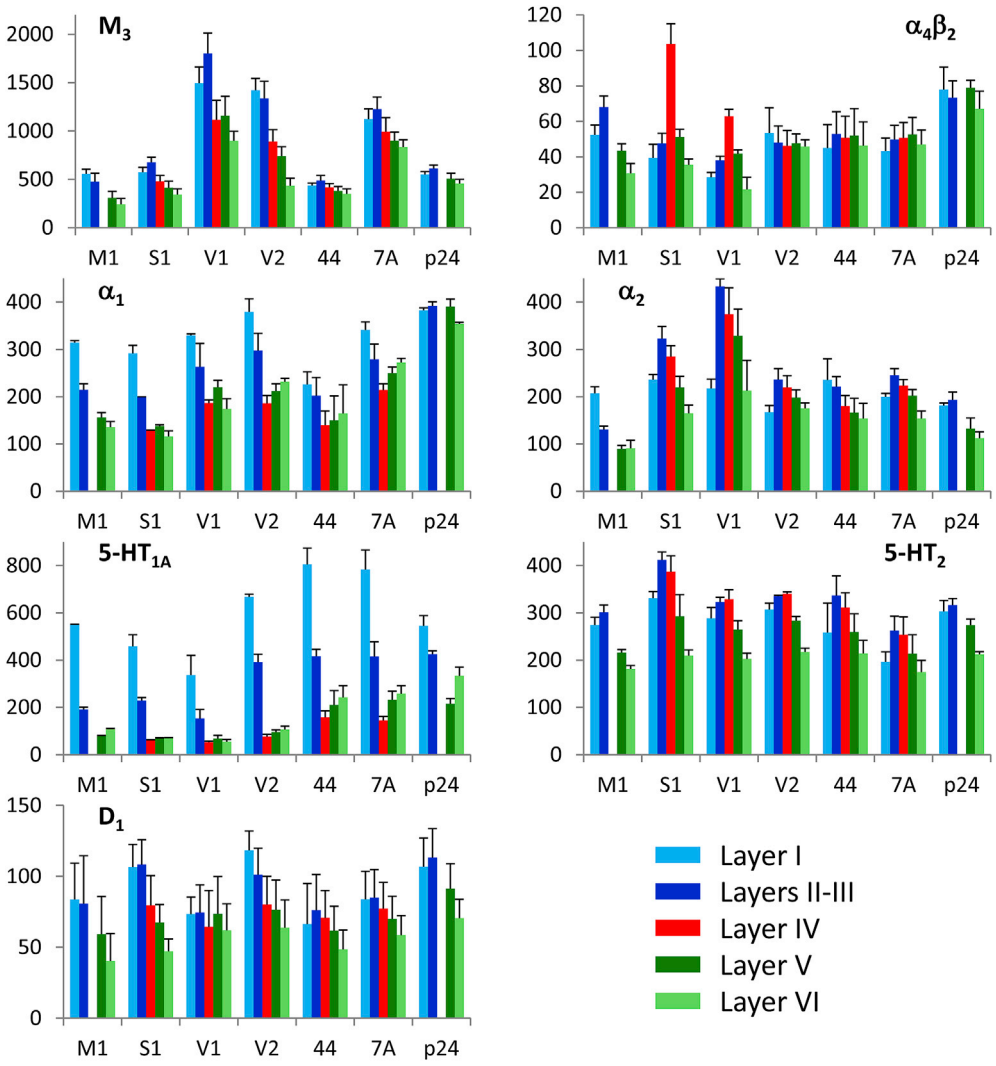

Fig. 17 (*continued*).

maximum in layer IV of primary sensory areas (S1, V1) and layer V of the limbic cortex (area p24). Furthermore, kainate receptors present three maxima in layers I, IIIc and V–VI of the multimodal association cortex (areas 7A, 44). Cholinergic nicotinic $\alpha_4\beta_2$ receptors reach the highest density in layer I of V2, nearly equally high densities in layers I and IIIc of areas 44 and 7A, in upper parts of layer III of M1, and in layer IV of S1 and V1. The laminar preference of the muscarinic M_2 receptors also shows distinct regional specificities with maximal densities in layers II–IIIa of M1, layers II–IIIc of the primary sensory areas (S1), two maxima in layers II–IVa and IVc-V of V1, no clear local preference in V2, a single sharp maximum in Layer V of area 44 and the limbic area p24, and a shallow maximum in layers IIIa-b of area 7A. In contrast, M_3 and M_1 receptor distributions are comparable throughout all isocortical areas, with the exception of M_1 densities in V1. Interestingly, although all layers of all cortical areas receive cholinergic innervation, regionally specific differences in the overall density of cholinergic axons, and in their lamination patterns have been demonstrated for the human brain (Mesulam et al., 1992; Mesulam, 2004).

The considerable regional variability in absolute densities is highlighted in Figs. 13–16. Despite this variable occurrence of receptors, some putative trends can be stated: the periarchicortical areas differ from the isocortical areas by absolute receptor densities and different laminar preferences of receptor maxima. Furthermore, primary sensory areas differ from secondary and multimodal association areas as well as from the motor cortex, which is clearly distinct from all other isocortical areas. This hierarchical aspect is demonstrated here only in the visual system, but may be applicable also to other sensory systems. E.g., hierarchical organization has also been shown in the somatosensory cortex by using neurochemical markers, i.e. cytochrome oxidase, acetylcholine-esterase, and NADPH-diaphorase (Eskenasy and Clarke, 2000). Presently it is not known whether these differences are caused by regionally distinct compositions of cortical layers, by the prevalence of different cell types within comparable layers, and/or by regional and layer specific microcircuitries or connectional features.

The distribution of muscarinic M_2 and M_3 receptors is not only layer- and sublayer-specific, but also shows a patchy distribution in primate V1 which is similar to patches with weak or strong cytochrome oxidase reactivity. Specifically, higher M_2 receptor densities are in register with the weakly reactive cytochrome oxidase interblob regions, whereas higher M_3 receptor densities coincide with the strongly reactive blob regions (Tigges et al., 1997).

4.3. White matter neurons (WMN)

In general, the border between layer VIb and the white matter is more clearly recognizable by the sudden decline of receptor densities in the white matter in receptor autoradiographs compared to cytoarchitectonic images. Therefore, the occasional appearance of spots of low receptor

densities in the white matter directly underlying the cortical ribbon is notable. The present careful comparison between neighboring cell body stained and receptor autoradiographically processed sections confirms that these spots are located in the white matter. Thus, we suggest that these spots of low receptor densities indicate contacts between WMNs and afferent axons. It is interesting, that this finding was visible in areas M1, S1, V2, 44, 7A, p34, but not in V1 or the entorhinal cortex, which also show sharp borders between the cortical ribbon and the white matter in cytoarchitectonic preparations. In most cases, excitatory glutamate receptors AMPA, NMDA, kainate and mGluR2/3 (arrows in Figs. 5, 6, 9–11) are found in the immediately adjacent white matter at a low concentration, often restricted to small spots. In some cases (arrows in Figs. 5, 6, 8–10), also patches of nicotinic $\alpha_4\beta_2$, $GABA_B$, M_1, M_2, M_3, α_1, α_2, 5-HT_{1A}, 5-HT_2, D_1, and A_1 receptors were seen. The occurrence of WMNs, which have cortico-cortical and cortico-thalamic connections, was recently demonstrated in frontal, temporal, and parietal association regions of the rhesus monkey (Mortazavi et al., 2016), as well as in the human supratemporal plane (Sacco et al., 2009). WMNs play an essential role during cortical development (Kanold and Luhmann, 2010; Wang et al., 2010), and persist at a decreased density postnatally (Kostovic and Rakic, 1980, 1990). It has been reported that they play a role in psychiatric disorders, since these are associated with altered density and distribution of WMNs (Connor et al., 2011; Joshi et al., 2012; Kostovic et al., 2011, 2014). It has been shown that WMNs express the muscarinic M_2 receptors, and are found more rarely in the primary visual and temporal cortex (García-Marin et al., 2010; Meyer et al., 1992; Smiley et al., 1998), but more frequently in frontal (e.g., M1), orbitofrontal (BA11), and cingulate areas. Here we reported for the first time multiple transmitter receptors with similar regional preference which may be associated with WMNs in the white matter underlying isocortical areas.

4.4. Comparison between calcium binding proteins and receptors in the islands

The lamination pattern of the entorhinal cortex obviously differs from that of isocortical areas. To emphasize this fact, we adhere to the nomenclature of classical descriptions of the entorhinal area (Braak, 1972; Rose, 1927; Sgonina, 1937), and use, e.g. the term Preα layer instead of layer II or Preβ instead of upper layer III as used in more recent publications (e.g. Beall and Lewis, 1992). A nomenclature with Roman numerals should be only used for the c-layers of the isocortex and not for allocortical structures.

The Preα and Preβ layers of the entorhinal cortex contain characteristic islands of nerve cells (verrucae gyri hippocampi; Retzius, 1896; Solodkin and Van Hoesen, 1996) which are never observed in the isocortex. The Preβ islands of the human and non-human primate brains are modular structures consisting of spiny stellate, pyramidal and non-pyramidal cells. The latter cell type of the entorhinal cortex was demonstrated in detail by parvalbumin and calbindin immunohistochemistry (Beall and Lewis, 1992). The calbindin-immunoreactive non-pyramidal neurons of these islands are visible to a different degree depending on subregions of the entorhinal cortex. Parvalbumin-immunoreactive non-pyramidal neurons of the islands are also locally distinct from calbindin-immunoreactive cells, and gradually increased in the more caudal part of the entorhinal cortex (Beall and Lewis, 1992). Moreover, parvalbumin-immunoreactive puncta were frequently found in the islands suggesting the presence of GABAergic synapses. It is presently not known whether these synapses in the entorhinal cortex are exclusively caused by local GABAergic interneurons, since parvalbumin-immunoreactive synapses from putative thalamo-cortical terminals have been demonstrated in the dorso-lateral prefrontal cortex of monkeys (Glausier et al., 2017; Lewis et al., 2001; Melchitzky et al., 1999). Since we could show here that metabotropic GluR2/3 receptors are found at intermediate to low densities in Preα and Preβ, also glutamatergic axons presumably of thalamo-cortical neurons may terminate in the islands.

A comparison between the various receptors studied here and the cytoarchitecture of the entorhinal cortex demonstrates distinct islands with a high density of 5-HT_{1A} receptors in Preβ. These islands also have relatively high $GABA_B$, M_1, and α_1, receptor densities. Contrastingly, the islands contain very few M_2 and α_2, receptors (Fig. 12). Moreover, some receptors (e.g., A_1, D_1) do not specifically label the islands. This indicates a considerable neurochemical heterogeneity of the islands in the entorhinal cortex and a putative innervation by GABA, acetylcholine, noradrenaline, and particularly serotonin which use specific receptors for signal processing.

4.5. Comparison between synaptic and receptor densities in the cortical ribbon

Although a concurrent synaptic and receptor development in the cerebral cortex has been proposed (Rakic et al., 1994), a comparison between laminar distribution of synapses and receptors must take into account the occurrence of synaptic and extrasynaptic receptor localizations. Nearly all studies on receptor localization have been performed in non-human primates and rodents. In general, all receptors studied in the present observations have been reported to be synaptically and extrasynaptically localized, but to a different degree in each receptor (Fuxe et al., 2012; Vizi et al., 2010). AMPA (Anggono and Huganir, 2012; Derkach et al., 2007), NMDA (Hardingham and Bading, 2010; Papouin and Oliet, 2014), kainate (Lerma, 2003), mGluR2/3 (Jin et al., 2016), $GABA_A$ (Fritschy and Brunig, 2003; Mortensen et al., 2011), $GABA_B$ (Pham et al., 1998), muscarinic (Groleau et al., 2015; Mrzljak et al., 1993), nicotinic (Posadas et al., 2013), α_1 (Mitrano et al., 2012), α_2 (Aoki et al., 1998), 5-HT_2 (Jansson et al., 2001), D_1 (Smiley et al., 1994), and adenosine (Abbracchio et al., 2009) receptors have been found with both localizations. A clear quantitative definition of the proportions between synaptic and extrasynaptic localizations is not available. Thus, correlations between receptor densities and number of synapses remain an approach with a caveat. Nevertheless, any correlation between synapses and receptors is helpful to speculate about the functional meaning of receptor densities. A further problem for this attempt is the methodical difficulty in measuring “true” synaptic numbers (DeFelipe et al., 1999; Huttenlocher and de Courten, 1987; Merchan-Perez et al., 2014; Roberts et al., 2015). However, the following discussion shows that despite all caveats regarding the methodical difficulties, surprising similarities between the laminar distribution patterns of synapses and receptor densities can be demonstrated.

In the primary visual cortex, highest synaptic densities are located in layers II–III (Huttenlocher and de Courten, 1987). Notably, highest densities of NMDA, mGluR2/3, A_1, $GABA_{A\ BZ}$, $GABA_B$, M_1, M_3, and 5-HT_2 receptors are also found in layers II–III of the primary visual cortex (Fig. 18). Best estimates of the laminar distribution pattern of synaptic densities are given by summarizing the receptor densities of $GABA_A$ and $GABA_B$ receptors, or by summarizing all glutamate receptors studied here (Fig. 18A). Interestingly, the majority of $GABA_A$ receptors expressed in the cerebral cortex are found in synapses, not in extrasynaptic sites (Fritschy and Brunig, 2003). Notably, these receptors are by far the most prevailing receptor types in V1, and reach highest absolute densities. Since the laminar distribution of glutamate and GABA receptor densities are most similar to the laminar distribution of synaptic density, we may speculate that the receptors labeled in autoradiographic experiments are mostly located at synapses, or in their immediate neighborhood.

Only the $GABA_A$ and nicotinic $\alpha_4\beta_2$ receptors reach the absolute highest densities in layer IVc (Fig. 18C, G); interestingly, the α_2 receptors have two maxima, the highest in layer IVa and a second in layer IVc (Fig. 18H), whereas the M_2 receptors reach highest densities in layers IVc and V (Fig. 18E). Thus, these four receptors are densely packed in the target layers IVa and IVc of the lateral geniculate input. A notable exception from the laminar pattern of most receptors is shown by the 5-HT_{1A} receptor, which reaches its absolute maximum in layer I (Fig. 18H).

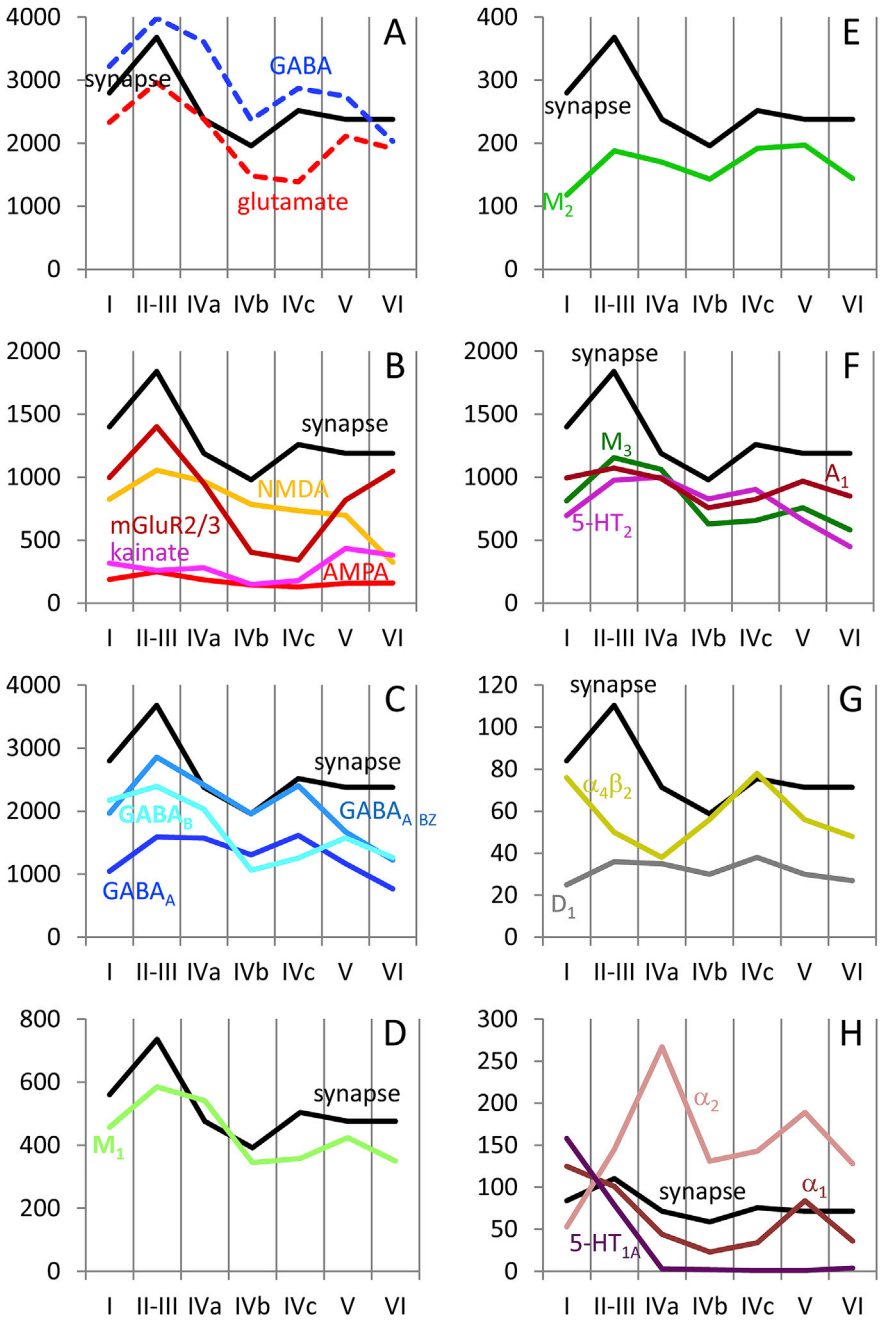

Fig. 18. Comparison of laminar synaptic and receptor densities in the human primary visual cortex. Synaptic densities were obtained from Huttenlocher and de Courten (1987), who expressed the original synapse counts in terms of synapses per 100 μm^2 area of section and then calculated the volume density of synapses, which we used in this figure. Synaptic profiles were stained with ethanolic phosphotungstic acid for electron microscopy. The errors of simple counting of synaptic profiles were corrected after De Hoff (1966) and Aghajanian and Bloom (1967). Receptor densities are calculated as mean value per layer from the data presented in Fig. 7 and 14. Note, y axis codes both for synaptic and receptor densities. Receptor densities are given in fmol/mg protein. Synaptic densities are given in n·10^5 (A and C), n·10^6 (E), n·2·10^6 (D), n·5·10^6 (B, F), or n·3·10^7 (G, H) synapses per mm^3.

Finally, the highest similarity in laminar patterns between synaptic density and that of a single receptor type is found for the $GABA_{A\ BZ}$ binding sites (Fig. 18C). Whereas nearly all receptors show a decline in their densities in layer VI, the kainate and mGluR2/3 receptors steeply increase from layer IVc to layers V–VI (Fig. 18B). Since particularly the mGluR2/3 receptors are very densely expressed in V1, their increase may explain the plateau of synaptic density from layer IVc to VI by compensating the decline of most other receptor types in these layers.

In summary, the comparison between synaptic and receptor densities indicates not only an interesting similarity of the laminar patterns of GABA and glutamate receptors with the synaptic density, but may provide an approach to study the neurochemical specificity of synaptic fields in the human primary visual cortex.

Acknowledgements

This project has received funding from the European Union's Horizon 2020 Framework Programme for Research and Innovation under Grant Agreement No 720270 (Human Brain Project SGA1).

References

Abbracchio, M.P., Burnstock, G., Verkhratsky, A., Zimmermann, H., 2009. Purinergic signalling in the nervous system: an overview. Trends Neurosci. 32, 19–29.

Aghajanian, G.K., Bloom, F.E., 1967. The formation of synaptic junctions in developing rat brain: a quantitative electron microscopic study. Brain Res. 6, 716–727.
Alonso-Nanclares, L., Gonzalez-Soriano, J., Rodriguez, J.R., DeFelipe, J., 2008. Gender differences in human cortical synaptic density. Proc. Natl. Acad. Sci. U. S. A. 105, 14615–14619.
Amaral, D.G., Price, J.L., 1984. Amygdalo-cortical projections in the monkey (*Macaca fascicularis*). J. Comp. Neurol. 230, 465–496.
Amunts, K., Lenzen, M., Friederici, A.D., Schleicher, A., Morosan, P., Palomero-Gallagher, N., Zilles, K., 2010. Broca's region: novel organizational principles and multiple receptor mapping. PLoS Biol. 8 http://dx.doi.org/10.1371/journal.pbio.1000489.
Amunts, K., Schleicher, A., Bürgel, U., Mohlberg, H., Uylings, H.B.M., Zilles, K., 1999. Broca's region revisited: cytoarchitecture and intersubject variability. J. Comp. Neurol. 412, 319–341.
Anggono, V., Huganir, R.L., 2012. Regulation of AMPA receptor trafficking and synaptic plasticity. Curr. Opin. Neurobiol. 22, 461–469.
Aoki, C., Venkatesan, C., Go, C.G., Forman, R., Kurose, H., 1998. Cellular and subcellular sites for noradrenergic action in the monkey dorsolateral prefrontal cortex as revealed by the immunocytochemical localization of noradrenergic receptors and axons. Cereb. Cortex 8, 269–277.
Bailey, P., von Bonin, G., 1951. The Isocortex of Man. University of Illinois Press, Urbana.
Baillarger, J.G.F., 1840. Recherches sur la structure de la couche corticale des circonvolutions du cervau. Mém. Acad. R. Méd. 8, 149–183.
Barbas, H., Garcia-Cabezas, M.A., 2015. Motor cortex layer 4: less is more. Trends Neurosci. 38, 259–261.
Beall, M.J., Lewis, D.A., 1992. Heterogeneity of layer II neurons in human entorhinal cortex. J. Comp. Neurol. 321, 241–266.
Berlin, R., 1858. Beitrag zur Strukturlehre der Grosshirnwindungen. Junge, Erlangen.
Braak, H., 1972. Pigmentarchitecture of the human cortex cerebri. I. Regio entorhinalis. Z Zellforsch Mikrosk Anat. 127, 407–438.
Braak, H., Braak, E., 1992. The human entorhinal cortex: normal morphology and lamina-specific pathology in various diseases. Neurosci. Res. 15, 6–31.
Brodmann, K., 1909. Vergleichende Lokalisationslehre der Großhirnrinde in ihren Prinzipien dargestellt auf Grund des Zellbaues. Barth, Leipzig.
Burkhalter, A., Bernardo, K.L., 1989. Organization of corticocortical connections in human visual cortex. Proc. Natl. Acad. Sci. U. S. A. 86, 1071–1075.
Callaghan, M.F., Freund, P., Draganski, B., Anderson, E., Cappelletti, M., Chowdhury, R., Diedrichsen, J., Fitzgerald, T.H., Smittenaar, P., Helms, G., Lutti, A., Weiskopf, N., 2014. Widespread age-related differences in the human brain microstructure revealed by quantitative magnetic resonance imaging. Neurobiol. Aging 35, 1862–1872.
Caspers, J., Palomero-Gallagher, N., Caspers, S., Schleicher, A., Amunts, K., Zilles, K., 2015. Receptor architecture of visual areas in the face and word-form recognition region of the posterior fusiform gyrus. Brain Struct. Funct. 220, 205–219.
Caspers, S., Schleicher, A., Bacha-Trams, M., Palomero-Gallagher, N., Amunts, K., Zilles, K., 2013. Organization of the human inferior parietal lobule based on receptor architectonics. Cereb. Cortex 23, 615–628.
Clarke, S., Miklossy, J., 1990. Occipital cortex in man: organization of callosal connections, related myelo- and cytoarchitecture, and putative boundaries of functional visual areas. J. Comp. Neurol. 298, 188–214.
Cohen-Adad, J., Polimeni, J.R., Helmer, K.G., Benner, T., McNab, J.A., Wald, L.L., Rosen, B.R., Mainero, C., 2012. T(2)* mapping and B(0) orientation-dependence at 7 T reveal cyto- and myeloarchitecture organization of the human cortex. NeuroImage 60, 1006–1014.
Connor, C.M., Crawford, B.C., Akbarian, S., 2011. White matter neuron alterations in schizophrenia and related disorders. Int. J. Dev. Neurosci. 29, 325–334.
Cortés, R., Probst, A., Palacios, J.M., 1987. Quantitative light microscopic autoradiographic localization of cholinergic muscarinic receptors in the human brain: forebrain. Neuroscience 20, 65–107.
Cortés, R., Probst, A., Tobler, H.J., Palacios, J.M., 1986. Muscarinic cholinergic receptor subtypes in the human brain. II. Quantitative autoradiographic studies. Brain Res. 362, 239–253.
De Hoff, R.T., 1966. Measurement of number and average size in volume. In: De Hoff, R.T., Rhines, F.N. (Eds.), Quantitative Microscopy. McGraw-Hill, New York, pp. 128–148.
DeFelipe, J., Marco, P., Busturia, I., Merchan-Perez, A., 1999. Estimation of the number of synapses in the cerebral cortex: methodological considerations. Cereb. Cortex 9, 722–732.
Deistung, A., Schafer, A., Schweser, F., Biedermann, U., Turner, R., Reichenbach, J.R., 2013. Toward in vivo histology: a comparison of quantitative susceptibility mapping (QSM) with magnitude-, phase-, and R2*-imaging at ultra-high magnetic field strength. NeuroImage 65, 299–314.
Derkach, V.A., Oh, M.C., Guire, E.S., Soderling, T.R., 2007. Regulatory mechanisms of AMPA receptors in synaptic plasticity. Nat. Rev. Neurosci. 8, 101–113.
Dick, F., Tierney, A.T., Lutti, A., Josephs, O., Sereno, M.I., Weiskopf, N., 2012. In vivo functional and myeloarchitectonic mapping of human primary auditory areas. J. Neurosci. 32, 16095–16105.
Dinse, J., Hartwich, N., Waehnert, M.D., Tardif, C.L., Schafer, A., Geyer, S., Preim, B., Turner, R., Bazin, P.L., 2015. A cytoarchitecture-driven myelin model reveals area-specific signatures in human primary and secondary areas using ultra-high resolution in-vivo brain MRI. NeuroImage 114, 71–87.
Eickhoff, S.B., Rottschy, C., Kujovic, M., Palomero-Gallagher, N., Zilles, K., 2008. Organizational principles of human visual cortex revealed by receptor mapping. Cereb. Cortex 18, 2637–2645.
Eickhoff, S.B., Schleicher, A., Scheperjans, F., Palomero-Gallagher, N., Zilles, K., 2007. Analysis of neurotransmitter receptor distribution patterns in the cerebral cortex. NeuroImage 34, 1317–1330.
Eskenasy, A.C., Clarke, S., 2000. Hierarchy within human SI: supporting data from cytochrome oxidase, acetylcholinesterase and NADPH-diaphorase staining patterns. Somatosens. Mot. Res. 17, 123–132.
Freese, J.L., Amaral, D.G., 2005. The organization of projections from the amygdala to visual cortical areas TE and V1 in the macaque monkey. J. Comp. Neurol. 486, 295–317.
Fritschy, J.M., Brunig, I., 2003. Formation and plasticity of GABAergic synapses: physiological mechanisms and pathophysiological implications. Pharmacol. Ther. 98, 299–323.
Fuxe, K., Borroto-Escuela, D.O., Romero-Fernandez, W., Diaz-Cabiale, Z., Rivera, A., Ferraro, L., Tanganelli, S., Tarakanov, A.O., Garriga, P., Narvaez, J.A., Ciruela, F., Guescini, M., Agnati, L.F., 2012. Extrasynaptic neurotransmission in the modulation of brain function. Focus on the striatal neuronal-glial networks. Front. Physiol. 3, 136.
Gallyas, F., 1979. Silver staining of myelin by means of physical development. Neurol. Res. 1, 203–209.
Garcia-Cabezas, M.A., Barbas, H., 2014. Area 4 has layer IV in adult primates. Eur. J. Neurosci. 39, 1824–1834.
García-Marin, V., Blazquez-Llorca, L., Rodriguez, J.R., Gonzalez-Soriano, J., DeFelipe, J., 2010. Differential distribution of neurons in the gyral white matter of the human cerebral cortex. J. Comp. Neurol. 518, 4740–4759.
Geyer, S., Weiss, M., Reimann, K., Lohmann, G., Turner, R., 2011. Microstructural parcellation of the human cerebral cortex - from Brodmann's post-mortem map to in vivo mapping with high-field magnetic resonance imaging. Front. Hum. Neurosci. 5, 19.
Glausier, J.R., Roberts, R.C., Lewis, D.A., 2017. Ultrastructural analysis of parvalbumin synapses in human dorsolateral prefrontal cortex. J. Comp. Neurol. 525, 2075–2089.
Graebenitz, S., Kedo, O., Speckmann, E.J., Gorji, A., Panneck, H., Hans, V., Palomero-Gallagher, N., Schleicher, A., Zilles, K., Pape, H.C., 2011. Interictal-like network activity and receptor expression in the epileptic human lateral amygdala. Brain 134, 2929–2947.
Groleau, M., Kang, J.I., Huppe-Gourgues, F., Vaucher, E., 2015. Distribution and effects of the muscarinic receptor subtypes in the primary visual cortex. Front. Synaptic Neurosci. 7, 10.
Hardingham, G.E., Bading, H., 2010. Synaptic versus extrasynaptic NMDA receptor signalling: implications for neurodegenerative disorders. Nat. Rev. Neurosci. 11, 682–696.
Hoyer, D., Pazos, A., Probst, A., Palacios, J.M., 1986a. Seroronin receptors in the human brain: II. Characterization and autoradiographic localization of 5-HT_{1C} and 5-HT_2 recognition sites. Brain Res. 376, 97–107.
Hoyer, D., Pazos, A., Probst, A., Palacios, J.M., 1986b. Serotonin receptors in the human brain: I. Characterization and autoradiographic localization of 5-HT_{1A} recognition sites. Apparent absence of 5-HT_{1B} recognition sites. Brain Res. 376, 85–86.
Huttenlocher, P.R., de Courten, Ch., 1987. The development of synapses in striate cortex of man. Hum. Neurobiol. 6, 1–9.
Jansen, K.L., Faull, R.L.M., Dragunow, M., 1989. Excitatory amino acid receptors in the human cerebral cortex: a quantitative autoradiographic study comparing the distributions of TCP, [^{3}H]glycine, L-[^{3}H]-glutamate, [^{3}H]AMPA and [^{3}H]kainic acid binding sites. Neuroscience 32, 587–607.
Jansson, A., Tinner, B., Bancila, M., Verge, D., Steinbusch, H.W., Agnati, L.F., Fuxe, K., 2001. Relationships of 5-hydroxytryptamine immunoreactive terminal-like varicosities to 5-hydroxytryptamine-2A receptor-immunoreactive neuronal processes in the rat forebrain. J. Chem. Neuroanat. 22, 185–203.
Jin, L.E., Wang, M., Yang, S.T., Yang, Y., Galvin, V.C., Lightbourne, T.C., Ottenheimer, D., Zhong, Q., Stein, J., Raja, A., Paspalas, C.D., Arnsten, A.F., 2016. mGluR2/3 mechanisms in primate dorsolateral prefrontal cortex: evidence for both presynaptic and postsynaptic actions. Mol. Psychiatry. http://dx.doi.org/10.1038/mp.2016.129.
Jones, E.G., 1986. Connectivity of the Primate Sensory-motor Cortex. Cerebral Cortex. Plenum, New York, pp. 113–183.
Jones, E.G., 1998. Viewpoint: the core and matrix of thalamic organization. Neuroscience 85, 331–345.
Joshi, D., Fung, S.J., Rothwell, A., Weickert, C.S., 2012. Higher gamma-aminobutyric acid neuron density in the white matter of orbital frontal cortex in schizophrenia. Biol. Psychiatry 72, 725–733.
Kanold, P.O., Luhmann, H.J., 2010. The subplate and early cortical circuits. Annu. Rev. Neurosci. 33, 23–48.
Kooijmans, R.N., Self, M.W., Wouterlood, F.G., Belien, J.A., Roelfsema, P.R., 2014. Inhibitory interneuron classes express complementary AMPA-receptor patterns in macaque primary visual cortex. J. Neurosci. 34, 6303–6315.
Kostovic, I., Jovanov-Milosevic, N., Rados, M., Sedmak, G., Benjak, V., Kostovic-Srzentic, M., Vasung, L., Culjat, M., Rados, M., Huppi, P., Judas, M., 2014. Perinatal and early postnatal reorganization of the subplate and related cellular compartments in the human cerebral wall as revealed by histological and MRI approaches. Brain Struct. Funct. 219, 231–253.
Kostovic, I., Judas, M., Sedmak, G., 2011. Developmental history of the subplate zone, subplate neurons and interstitial white matter neurons: relevance for schizophrenia. Int. J. Dev. Neurosci. 29, 193–205.
Kostovic, I., Rakic, P., 1980. Cytology and time of origin of interstitial neurons in the white matter in infant and adult human and monkey telencephalon. J. Neurocytol. 9, 219–242.
Kostovic, I., Rakic, P., 1990. Developmental history of the transient subplate zone in the visual and somatosensory cortex of the macaque monkey and human brain. J. Comp. Neurol. 297, 441–470.
la Fougère, C., Grant, S., Kostikov, A., Schirrmacher, R., Gravel, P., Schipper, H.M., Reader, A., Evans, A., Thiel, A., 2011. Where in-vivo imaging meets

cytoarchitectonics: the relationship between cortical thickness and neuronal density measured with high-resolution [^{18}F]flumazenil-PET. NeuroImage 56, 951–960.
Lashley, K.S., Clark, G., 1946. The cytoarchitecture of the cerebral cortex of Ateles; a critical examination of architectonic studies. J. Comp. Neurol. 85, 223–305.
Lerma, J., 2003. Roles and rules of kainate receptors in synaptic transmission. Nat. Rev. Neurosci. 4, 481–495.
Lewis, D.A., Cruz, D.A., Melchitzky, D.S., Pierri, J.N., 2001. Lamina-specific deficits in parvalbumin-immunoreactive varicosities in the prefrontal cortex of subjects with schizophrenia: evidence for fewer projections from the thalamus. Am. J. Psychiatry 158, 1411–1422.
Livingstone, M.S., Hubel, D.H., 1987. Connections between layer 4B of area 17 and the thick cytochrome oxidase stripes of area 18 in the squirrel monkey. J. Neurosci. 7, 3371–3377.
Lund, J.S., Yoshio, Levitt, J.B., 1994. Substrates for Interlaminar Conncetions in Area V1 of Macaque Monkey Cerebral Cortex. Cerebral Cortex. Plenum, New York, pp. 37–60.
Marques, J.P., Khabipova, D., Gruetter, R., 2017. Studying cyto and myeloarchitecture of the human cortex at ultra-high field with quantitative imaging: R1, R2* and magnetic susceptibility. NeuroImage 147, 152–163.
Megías, M., Emri, Z., Freund, T.F., Gulyás, A.I., 2001. Total number and distribution of inhibitory and excitatory synapses on hippocampal CA1 pyramidal cells. Neuroscience 102, 527–540.
Melchitzky, D.S., Sesack, S.R., Lewis, D.A., 1999. Parvalbumin-immunoreactive axon terminals in macaque monkey and human prefrontal cortex: laminar, regional, and target specificity of type I and type II synapses. J. Comp. Neurol. 408, 11–22.
Merchan-Perez, A., Rodriguez, J.R., Gonzalez, S., Robles, V., DeFelipe, J., Larranaga, P., Bielza, C., 2014. Three-dimensional spatial distribution of synapses in the neocortex: a dual-beam electron microscopy study. Cereb. Cortex 24, 1579–1588.
Merker, B., 1983. Silver staining of cell bodies by means of physical development. J. Neurosci. Methods 9, 235–241.
Mesulam, M.M., 2004. The cholinergic innervation of the human cerebral cortex. Prog. Brain Res. 145, 67–78.
Mesulam, M.M., Hersh, L.B., Mash, D.C., Geula, C., 1992. Differential cholinergic innervation within functional subdivisions of the human cerebral cortex: a choline acetyltransferase study. J. Comp. Neurol. 318, 316–328.
Meyer, G., Wahle, P., Castaneyra-Perdomo, A., Ferres-Torres, R., 1992. Morphology of neurons in the white matter of the adult human neocortex. Exp. Brain Res. 88, 204–212.
Mitrano, D.A., Schroeder, J.P., Smith, Y., Cortright, J.J., Bubula, N., Vezina, P., Weinshenker, D., 2012. Alpha-1 adrenergic receptors are localized on presynaptic elements in the nucleus accumbens and regulate mesolimbic dopamine transmission. Neuropsychopharmacology 37, 2161–2172.
Mohan, H., Verhoog, M.B., Doreswamy, K.K., Eyal, G., Aardse, R., Lodder, B.N., Goriounova, N.A., Asamoah, B., AB, B.B., Groot, C., van der Sluis, S., Testa-Silva, G., Obermayer, J., Boudewijns, Z.S., Narayanan, R.T., Baayen, J.C., Segev, I., Mansvelder, H.D., de Kock, C.P., 2015. Dendritic and axonal architecture of individual pyramidal neurons across layers of adult human neocortex. Cereb. Cortex 25, 4839–4853.
Morosan, P., Rademacher, J., Palomero-Gallagher, N., Zilles, K., 2005. Anatomical organization of the human auditory cortex: cytoarchitecture and transmitter receptors. In: Heil, P., König, E., Budinger, E. (Eds.), Auditory Cortex – towards a Synthesis of Human and Animal Research. Lawrence Erlbaum, Mahwah, New Jersey, pp. 27–50.
Mortazavi, F., Wang, X., Rosene, D.L., Rockland, K.S., 2016. White matter neurons in young adult and aged rhesus monkey. Front. Neuroanat. 10, 15.
Mortensen, M., Patel, B., Smart, T.G., 2011. GABA potency at GABA$_A$ receptors found in synaptic and extrasynaptic zones. Front. Cell Neurosci. 6, 1.
Mrzljak, L., Levey, A.I., Goldman-Rakic, P.S., 1993. Association of m1 and m2 muscarinic receptor proteins with asymmetric synapses in the primate cerebral cortex: morphological evidence for cholinergic modulation of excitatory neurotransmission. Proc. Natl. Acad. Sci. U. S. A. 90, 5194–5198.
Palomero-Gallagher, N., Amunts, K., Zilles, K., 2015. Transmitter receptor distribution in the human brain. In: Toga, A.W. (Ed.), Brain Mapping: an Encyclopedic Reference. Academic Press: Elsevier, San Diego, pp. 261–275.
Palomero-Gallagher, N., Mohlberg, H., Zilles, K., Vogt, B.A., 2008. Cytology and receptor architecture of human anterior cingulate cortex. J. Comp. Neurol. 508, 906–926.
Palomero-Gallagher, N., Schleicher, A., Bidmon, H.J., Pannek, H.W., Hans, V., Gorji, A., Speckmann, E.J., Zilles, K., 2012. Multireceptor analysis in human neocortex reveals complex alterations of receptor ligand binding in focal epilepsies. Epilepsia 53, 1987–1997.
Palomero-Gallagher, N., Vogt, B.A., Schleicher, A., Mayberg, H.S., Schleicher, A., Zilles, K., 2009. Receptor architecture of human cingulate cortex: evaluation of the four-region neurobiological model. Hum. Brain Mapp. 30, 2336–2355.
Palomero-Gallagher, N., Zilles, K., 2017. Cyto- and receptorarchitectonic mapping of the human brain. In: Huitinga, I., Webster, M. (Eds.), Brain Banking Neurological and Psychiatric Disorders. Elsevier.
Palomero-Gallagher, N., Zilles, K., Schleicher, A., Vogt, B.A., 2013. Cyto- and receptor architecture of area 32 in human and macaque brains. J. Comp. Neurol. 521, 3272–3286.
Papouin, T., Oliet, S.H., 2014. Organization, control and function of extrasynaptic NMDA receptors. Philos. Trans. R. Soc. Lond. Ser. B Biol. Sci. 369, 20130601.
Pazos, A., Probst, A., Palacios, J.M., 1987a. Serotonin receptors in the human brain. III. Autoradiographic mapping of serotonin-1 receptors. Neuroscience 21, 97–122.
Pazos, A., Probst, A., Palacios, J.M., 1987b. Serotonin receptors in the human brain. IV. Autoradiographic mapping of serotonin-2 receptors. Neuroscience 21, 123–139.
Peters, A., 1994. The Organization of the Primary Visual Cortex in the Macaque. Cerebral Cortex. Plenum, New York, pp. 1–35.
Pham, T.M., Nurse, S., Lacaille, J.C., 1998. Distinct GABA$_B$ actions via synaptic and extrasynaptic receptors in rat hippocampus in vitro. J. Neurophysiol. 80, 297–308.
Polimeni, J.R., Fischl, B., Greve, D.N., Wald, L.L., 2010. Laminar analysis of 7T BOLD using an imposed spatial activation pattern in human V1. NeuroImage 52, 1334–1346.
Posadas, I., Lopez-Hernandez, B., Cena, V., 2013. Nicotinic receptors in neurodegeneration. Curr. Neuropharmacol. 11, 298–314.
Rakic, P., Bourgeois, J.P., Goldman-Rakic, P.S., 1994. Synaptic development of the cerebral cortex: implications for learning, memory, and mental illness. Prog. Brain Res. 102, 227–243.
Reiner, A., Jiao, Y., Del, M.N., Laverghetta, A.V., Lei, W.L., 2003. Differential morphology of pyramidal tract-type and intratelencephalically projecting-type corticostriatal neurons and their intrastriatal terminals in rats. J. Comp. Neurol. 457, 420–440.
Retzius, G., 1896. Das Menschenhirn. Studien in der makroskopischen Morphologie. Norstedt Soner, Stockholm.
Roberts, R.C., Barksdale, K.A., Roche, J.K., Lahti, A.C., 2015. Decreased synaptic and mitochondrial density in the postmortem anterior cingulate cortex in schizophrenia. Schizophr. Res. 168, 543–553.
Rockland, K.S., 1994. The Organization of Feedback Connections from Area V2 (18) to V1 (17). Cerebral Cortex. Plenum, New York, pp. 261–299.
Rose, M., 1927. Die sog. Riechrinde beim menschen und beim Affen. II. Teil des “Allocortex bei Tier und Mensch”. J. Psychol. Neurol. 32, 97–160.
Rubio-Garrido, P., Perez-de-Manzo, F., Porrero, C., Galazo, M.J., Clasca, F., 2009. Thalamic input to distal apical dendrites in neocortical layer 1 is massive and highly convergent. Cereb. Cortex 19, 2380–2395.
Sacco, C.B., Tardif, E., Genoud, C., Probst, A., Tolnay, M., Janzer, R.C., Verney, C., Kraftsik, R., Clarke, S., 2009. GABA receptor subunits in human auditory cortex in normal and stroke cases. Acta Neurobiol. Exp. Wars. 69, 469–493.
Sanides, F., 1962. Die Architektonik des menschlichen Stirnhirns. Springer, Berlin, Göttingen, Heidelberg.
Sanides, F., 1964. The cyto-myeloarchitecture of the human frontal lobe and its relation to phylogenetic differentiation of the cerebral cortex. J. Hirnforsch. 7, 269–282.
Scheperjans, F., Grefkes, C., Palomero-Gallagher, N., Schleicher, A., Zilles, K., 2005a. Subdivisions of human parietal area 5 revealed by quantitative receptor autoradiography: a parietal region between motor, somatosensory and cingulate cortical areas. NeuroImage 25, 975–992.
Scheperjans, F., Hermann, K., Eickhoff, S.B., Amunts, K., Schleicher, A., Zilles, K., 2008. Observer-independent cytoarchitectonic mapping of the human superior parietal cortex. Cereb. Cortex 18, 846–867.
Scheperjans, F., Palomero-Gallagher, N., Grefkes, C., Schleicher, A., Zilles, K., 2005b. Transmitter receptors reveal segregation of cortical areas in the human superior parietal cortex: relations to visual and somatosensory regions. NeuroImage 28, 362–379.
Schleicher, A., Amunts, K., Geyer, S., Kowalski, T., Schormann, T., Palomero-Gallagher, N., Zilles, K., 2000. A stereological approach to human cortical architecture: identification and delineation of cortical areas. J. Chem. Neuroanat. 20, 31–47.
Schleicher, A., Palomero-Gallagher, N., Morosan, P., Eickhoff, S.B., Kowalski, T., de Vos, K., Amunts, K., Zilles, K., 2005. Quantitative architectural analysis: a new approach to cortical mapping. Anat. Embryol. 210, 373–386.
Segraves, M.A., Rosenquist, A.C., 1982. The distribution of the cells of origin of callosal projections in cat visual cortex. J. Neurosci. 2, 1079–1089.
Sgonina, K., 1937. Zur vergleichenden Anatomie der Entorhinal- und Präsubikularregion. J. Psychol. Neurol. 48, 56–163.
Shipp, S., 2007. Structure and function of the cerebral cortex. Curr. Biol. 17, R443–R449.
Smiley, J.F., Levey, A.I., Ciliax, B.J., Goldman-Rakic, P.S., 1994. D$_1$ dopamine receptor immunoreactivity in human and monkey cerebral cortex: predominant and extrasynaptic localization in dendritic spines. Proc. Natl. Acad. Sci. U. S. A. 91, 5720–5724.
Smiley, J.F., Levey, A.I., Mesulam, M.M., 1998. Infracortical interstitial cells concurrently expressing m2-muscarinic receptors, acetylcholinesterase and nicotinamide adenine dinucleotide phosphate-diaphorase in the human and monkey cerebral cortex. Neuroscience 84, 755–769.
Solodkin, A., Van Hoesen, G.W., 1996. Entorhinal cortex modules of the human brain. J. Comp. Neurol. 365, 610–617.
Stephan, H., 1975. Allocortex. Springer, Berlin.
Tardif, E., Clarke, S., 2001. Intrinsic connectivity of human auditory areas: a tracing study with DiI. Eur. J. Neurosci. 13, 1045–1050.
Tardif, E., Probst, A., Clarke, S., 2007. Laminar specificity of intrinsic connections in Broca's area. Cereb. Cortex 17, 2949–2960.
Tigges, M., Tigges, J., Rees, H., Rye, D., Levey, A.I., 1997. Distribution of muscarinic cholinergic receptor proteins m1 to m4 in area 17 of normal and monocularly deprived rhesus monkeys. J. Comp. Neurol. 388, 130–145.
Vizi, E.S., Fekete, A., Karoly, R., Mike, A., 2010. Non-synaptic receptors and transporters involved in brain functions and targets of drug treatment. Br. J. Pharmacol. 160, 785–809.
Vogt, B.A., Hof, P.R., Zilles, K., Vogt, L.J., Herold, C., Palomero-Gallagher, N., 2013. Cingulate area 32 homologies in mouse, rat, macaque and human: cytoarchitecture and receptor architecture. J. Comp. Neurol. 521, 4189–4204.
Vogt, B.A., Pandya, D.N., 1978. Cortico-cortical connections of somatic sensory cortex (areas 3, 1 and 2) in the rhesus monkey. J. Comp. Neurol. 177, 179–191.
Vogt, C., Vogt, O., 1919. Allgemeinere ergebnisse unserer Hirnforschung. J. Psychol. Neurol. 25, 279–462.
Vogt, O., 1911. Die Myeloarchitektonik des Isocortex parietalis. J. Psychol. Neurol. 18, 379–396.

von Economo, C., Koskinas, G.N., 1925. Die Cytoarchitektonik der Hirnrinde des erwachsenen Menschen. Springer, Wien, Berlin.
Wang, W.Z., Hoerder-Suabedissen, A., Oeschger, F.M., Bayatti, N., Ip, B.K., Lindsay, S., Supramaniam, V., Srinivasan, L., Rutherford, M., Mollgard, K., Clowry, G.J., Molnar, Z., 2010. Subplate in the developing cortex of mouse and human. J. Anat. 217, 368–380.
Wilson, C.J., 1987. Morphology and synaptic connections of crossed corticostriatal neurons in the rat. J. Comp. Neurol. 263, 567–580.
Zilles, K., Amunts, K., 2009. Receptor mapping: architecture of the human cerebral cortex. Curr. Opin. Neurol. 22, 331–339.
Zilles, K., Amunts, K., 2015. Anatomical basis for functional specialization. In: Uludag, K., Ugurbil, K., Berliner, L. (Eds.), fMRI: from Nuclear Spins to Brain Functions. Springer, New York, pp. 27–66.
Zilles, K., Bacha-Trams, M., Palomero-Gallagher, N., Amunts, K., Friederici, A.D., 2015a. Common molecular basis of the sentence comprehension network revealed by neurotransmitter receptor fingerprints. Cortex 63, 79–89.
Zilles, K., Clarke, S., 1997. Architecture, connectivity, and transmitter receptors of human extrastriate visual cortex. Comparison with nonhuman primates. Cereb. Cortex 12, 673–742.
Zilles, K., Palomero-Gallagher, N., 2001. Cyto-, myelo-, and receptor architectonics of the human parietal cortex. NeuroImage 14, S8–S20.
Zilles, K., Palomero-Gallagher, N., 2017. Comparative analysis of receptor types that identify primary cortical sensory areas. In: Kaas, J.H. (Ed.), Evolution of Nervous Systems, second ed. Elsevier, Oxford, pp. 225–245.
Zilles, K., Palomero-Gallagher, N., Amunts, K., 2015b. Myeloarchitecture and maps of the cerebral cortex. In: Toga, A.W. (Ed.), Brain Mapping: an Encyclopedic Reference. Elsevier, pp. 137–156.
Zilles, K., Palomero-Gallagher, N., Grefkes, C., Scheperjans, F., Boy, C., Amunts, K., Schleicher, A., 2002a. Architectonics of the human cerebral cortex and transmitter receptor fingerprints: reconciling functional neuroanatomy and neurochemistry. Eur. Neuropsychopharmacol. 12, 587–599.
Zilles, K., Palomero-Gallagher, N., Schleicher, A., 2004. Transmitter receptors and functional anatomy of the cerebral cortex. J. Anat. 205, 417–432.
Zilles, K., Qü, M., Köhling, R., Speckmann, E.J., 1999. Ionotropic glutamate and GABA receptors in human epileptic neocortical tissue: quantitative *in vitro* receptor autoradiography. Neuroscience 94, 1051–1061.
Zilles, K., Schleicher, A., Palomero-Gallagher, N., Amunts, K., 2002b. Quantitative analysis of cyto- and receptorarchitecture of the human brain. In: Toga, A.W., Mazziotta, J.C. (Eds.), Brain Mapping. The Methods, second ed. Elsevier, Amsterdam, pp. 573–602.